Dependence of Contextual Modulation in Macaque V1 on Interlaminar Signal Flow

Shude Zhu[1], Yu Jin Oh[1], Ethan B. Trepka[1], Xiaomo Chen[1,2], Tirin Moore[1*]

Author affiliations:

[1]Department of Neurobiology and Howard Hughes Medical Institute, Stanford University School of Medicine, Stanford, CA 94305, USA.

[2]Center for Neuroscience, Department of Neurobiology, Physiology, and Behavior, UC Davis, Davis, CA 95618, USA.

***Correspondence:** tirin@stanford.edu

Abstract

In visual cortex, neural correlates of subjective perception can be generated by modulation of activity from beyond the classical receptive field (CRF). In macaque V1, activity generated by nonclassical receptive field (nCRF) stimulation involves different intracortical circuitry than activity generated by CRF stimulation, suggesting that interactions between neurons across V1 layers differ under CRF and nCRF stimulus conditions. Using Neuropixels probes, we measured border ownership modulation within large, local populations of V1 neurons. We found that neurons in single columns preferred the same side of objects located outside of the CRF. In addition, we found that cross-correlations between pairs of neurons situated across feedback/horizontal and input layers differed between CRF and nCRF stimulation. Furthermore, independent of the comparison with CRF stimulation, we observed that the magnitude of border ownership modulation increased with the proportion of information flow from feedback/horizontal layers to input layers. These results demonstrate that the flow of signals between layers covaries with the degree to which neurons integrate information from beyond the CRF.

Introduction

The classical receptive field (CRF) defines the region of the sensory periphery where appropriate stimulation evokes a spiking response in a neuron (Hartline, 1938, Alonso and Chen, 2009). Those evoked responses are largely driven by feedforward inputs from earlier stages of sensory processing. In macaque primary visual cortex (V1), neuronal activity is largely determined by ascending input from the dorsal lateral geniculate nucleus (dLGN) which arrives principally in layers 4Cα, 4Cβ and 6 (Hubel and Wiesel, 1972, Hendrickson et al., 1978, Blasdel and Lund, 1983, Callaway, 1998, Callaway, 2004). However, considerable evidence has established that the responses of sensory cortical neurons are also robustly influenced by stimulation concurrently presented outside of the CRF (Allman et al., 1985, Fitzpatrick, 2000, Albright and Stoner, 2002, Roelfsema, 2006, Angelucci et al., 2017). Specifically, whereas stimulation outside of the CRF alone fails to evoke spiking responses, such stimulation nonetheless alters the responses evoked by stimulation within the CRF. In the visual cortex, these nonclassical receptive field (nCRF) effects often contribute to the neural correlates of visual perceptual phenomena, such as illusory contours (von der Heydt et al., 1984, Ramsden et al., 2001), visual salience and boundary segmentation (Knierim and van Essen, 1992, Sillito et al., 1995, Yan et al., 2018, Lee et al., 2002, Nothdurft et al., 1999), contour integration (Nelson and Frost, 1985, Kapadia et al., 1995, Li et al., 2006), figure-ground segregation (Lamme, 1995, Zipser et al., 1996, Poort et al., 2012), and border ownership (Zhou et al., 2000, von der Heydt, 2015, von der Heydt, 2023).

In contrast to the feedforward mechanisms underlying the CRF, nCRF effects are thought to be generated either by feedback from neurons with larger CRFs in higher areas (Hupe et al., 1998, Bullier et al., 2001, Bair et al., 2003, Nassi et al., 2013, Chen et al., 2017, Klink et al., 2017, Zhang et al., 2014, Nurminen et al., 2018, Keller et al., 2020, Pak et al., 2020, Vangeneugden et

52 al., 2019, Gieselmann and Thiele, 2022, Chen et al., 2014, van Kerkoerle et al., 2014), or through
53 intracortical horizontal connections (Adesnik et al., 2012, Chisum et al., 2003, Stettler et al., 2002),
54 or by both (Angelucci and Bressloff, 2006, Schwabe et al., 2006, Ichida et al., 2007, Angelucci et
55 al., 2017, Liang et al., 2017, Self et al., 2013). In contrast to feedforward inputs, feedback and
56 horizontal inputs to V1 both avoid layer 4C and terminate predominantly in superficial and deep
57 layers (Rockland and Lund, 1983, Rockland and Pandya, 1979, Rockland and Virga, 1989,
58 Anderson and Martin, 2009, Markov et al., 2014, Federer et al., 2021, Gilbert and Wiesel, 1983,
59 Shmuel et al., 2005, Siu et al., 2021). These differences between feedforward and
60 feedback/horizontal circuitry suggest that the flow of signals across V1 layers should covary with
61 the type of visual stimulation.

62 Newly developed, high-density Neuropixels probes have enabled recordings from a large,
63 dense population of neurons (Jun et al., 2017, Trautmann et al., 2023), and dramatically increase
64 the quantity of identifiable functional interactions between pairs of neurons, particularly in non-
65 human primates (Trepka et al., 2022). Recently, this approach was used to recapitulate known
66 circuit properties, such as the pairwise lead-lag relationship between simple and complex cells and
67 the canonical laminar input-output relationship in macaque V1 (Trepka et al., 2022), as well as the
68 visual hierarchy in mouse visual cortical (Siegle et al., 2021, Jia et al., 2022) and subcortical areas
69 (Sibille et al., 2022).

70 Here, using Neuropixels probes, we recorded the activity of hundreds of neurons
71 simultaneously from single V1 columns in anesthetized macaques during CRF and nCRF
72 stimulation. We leveraged the high yields obtained from different layers to examine the
73 organization and circuitry underlying contextual modulation, specifically border ownership (B_{own}).
74 B_{own} is a form of contextual modulation in which neurons signal the occluding border between the

75 background and a foreground object using stimulus information beyond the CRF. This function
76 appears to be crucial for natural scene segmentation and object recognition (Nakayama et al.,
77 1995). It has been shown that many neurons in early visual areas, including V1, respond differently
78 to identical edges (borders) of objects when those objects lie at different locations outside the CRFs
79 (Zhou et al., 2000, Franken and Reynolds, 2021, Hesse and Tsao, 2016, Hesse and Tsao, 2023).
80 B_{own} emerges rapidly after visual response onset (Sugihara et al., 2011), yet the relative
81 contributions of feedforward, feedback, and horizontal circuits to B_{own} remain unknown. Also
82 unknown is whether B_{own} is present under anesthesia. Several other types of contextual modulation
83 have been demonstrated in anesthetized animals (Ramsden et al., 2001, Hupe et al., 1998, Bair et
84 al., 2003, Allman et al., 1985, Gilbert and Wiesel, 1990, Nothdurft et al., 1999, Webb et al., 2003,
85 Zarella and Ts'o, 2016, Muller et al., 2003, Henry et al., 2013, Bijanzadeh et al., 2018, although
86 see Lamme et al., 1998) and can involve inter-cortical feedback (Nurminen et al., 2018). Moreover,
87 B_{own} has been shown to occur independently of attention (Qiu et al., 2007, O'Herron and von der
88 Heydt, 2009), and before object shape recognition (Williford and von der Heydt, 2016, Ko and
89 von der Heydt, 2018), suggesting it may not rely on higher cognitive control or object recognition
90 areas. Rather, B_{own} may emerge through pre-attentive, automatic grouping mechanism in
91 low/middle level visual areas, signifying a representation of “proto-objects” in the early visual
92 cortex (von der Heydt, 2015, von der Heydt, 2023, Self et al., 2019).

Results

Classical RF stimulation in single V1 columns

Neuronal activity was recorded from two anesthetized rhesus macaques (M1 and M2, *Macaca mulatta*) using high-density, multi-contact Neuropixels probes (version 3A, IMEC Inc., Belgium) (Figure 1A) (Methods). These animals had no prior experience with awake experiments or exposure to the stimuli used in this study. Neuropixels probes were inserted into the lateral operculum of V1 with the aid of a surgical microscope at angles nearly perpendicular to the cortical surface. Prior to insertion, the probes were coated with a DiI derivative for subsequent histological visualization of the tracks (Methods) (Supplementary Figure S1). Four Neuropixels probe penetrations were made either in the opercular surface (M1, *pen 1-2*, ~4-6° eccentricities) or within the underlying calcarine sulcus (M2, *pen 3-4*, ~6-10° eccentricities) using the programmable channel selection feature of the Neuropixels probe. The boundaries of laminar compartments were estimated by combining current-source density (CSD) measurements and histological data (Figure 1B; Supplementary Figure S1) (Methods). Each recorded neuron was assigned to one of four laminar compartments, specifically 5/6, 4C, 4A/B, 2/3 (mean thickness: 489, 281, 311, 650 µm, respectively, consistent with previous anatomical (O'Kusky and Colonnier, 1982, Lund, 1973) and CSD (Self et al., 2013, Chen et al., 2017) studies). We measured the responses from a total of 677 visually driven neurons (N = 159, 181, 210, and 127 per recording) to classical receptive field (CRF) stimulation, and 621 neurons (N = 142, 179, 152, and 148 per recording) to nonclassical

receptive field (nCRF) stimulation (Methods). As a result of the nearly perpendicular penetrations, the visual CRFs of V1 neurons were largely overlapping across the cortical depth (Figure 1C).

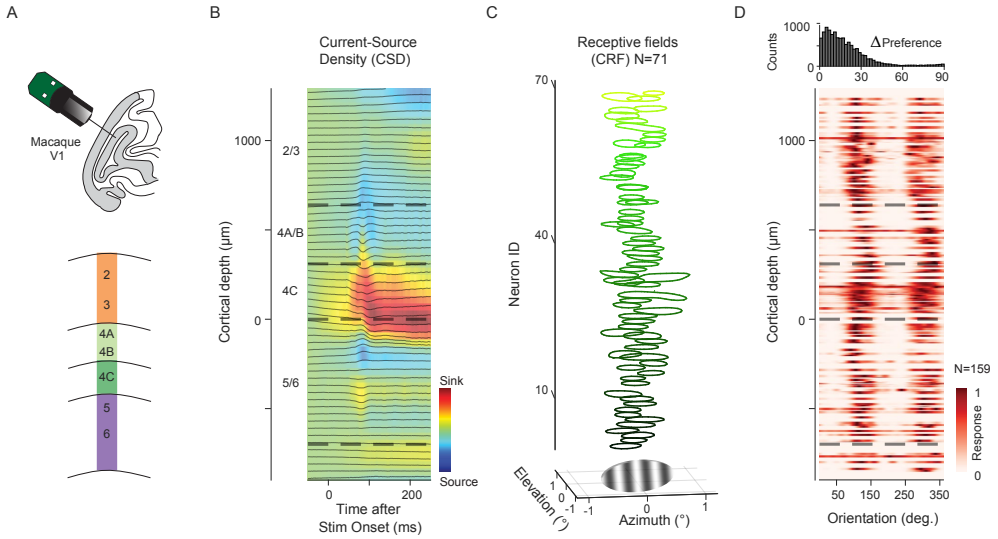

Figure 1. Classical receptive field (CRF) stimulation in single V1 columns. (A) Neuropixels probe (384 channels/3.84mm) penetrations made into the lateral surface or underlying calcarine sulcus of macaque V1. Bottom: Diagram of designated laminar compartments. (B) Current-Source density (CSD) profile from an example recording session (M1, *pen1*), showing the early current sink (red) indicative of layer 4C. Laminar compartment boundaries (dashed lines) were determined using histological data and the CSD profile. (C) Top: 71 well-defined classical receptive fields (CRF) vertically stacked along the cortical depth, mapped with a 10 x 10 array (4 x 4 dva) of probe stimuli (gratings, 0.4 dva in diameter). Bottom: Drifting Gabor grating (1.5 dva in diameter) used for CRF stimulation, positioned within the joint receptive fields of recorded neurons. (D) Heatmap of visual responses from 159 neurons to 36 drift directions of Gabor gratings, vertically stacked along cortical depth (M1, *pen1*). Top: Distribution of differences in preferred orientation for all pairwise combinations of neurons.

During each recording session, neurons were first tested with CRF stimuli consisting of drifting Gabor gratings with 1.5 degrees of visual angle (dva) in diameter, presented at the joint CRF location of simultaneously recorded neurons (Methods). In each of the four recordings, neurons across cortical depth exhibited very similar preferences to grating orientations (Figure 1D). The modal pairwise difference in preferred orientation between neurons across layers was near zero (*pen1* = 5°; *pen2* = 5°; *pen3* = 1°; *pen4* = 1°). This result confirmed that our recordings were nearly perpendicular and included neurons predominantly from single orientation columns.

121 Gratings were sized to largely restrict the stimuli within the CRFs of recorded neurons to maximize
122 the extent to which V1 responses were driven in large proportion by feedforward circuitry. In V1,
123 geniculocortical inputs initially drive neurons within layers 4Cα, 4Cβ, and layer 6 (Hubel and
124 Wiesel, 1972, Hendrickson et al., 1978, Blasdel and Lund, 1983), which then propagate to
125 supragranular and infragranular layers (Callaway, 1998, Callaway, 2004).
126

127 **Nonclassical RF stimulation and border ownership**

128 Within each of the recordings, we also examined the responses of V1 neurons to nCRF stimuli. It
129 is known that neurons in primate visual cortex integrate visual information from far beyond their
130 CRFs (Albright and Stoner, 2002, Allman et al., 1985, Fitzpatrick, 2000, Roelfsema, 2006,
131 Angelucci et al., 2017). One example of contextual modulation is the selectivity of neurons to
132 border ownership (B_{own}). Specifically, neurons in early visual areas respond differently to identical
133 edges (borders) of objects when those objects lie at different locations outside the CRFs (Zhou et
134 al., 2000, Franken and Reynolds, 2021, Hesse and Tsao, 2016, Hesse and Tsao, 2023) (Figure 2).
135 As with other forms of nCRF modulation, B_{own} is thought to emerge either by feedback from higher
136 areas (Craft et al., 2007, Jehee et al., 2007, Layton et al., 2012, Eguchi and Stringer, 2016,
137 Wagatsuma et al., 2021, Mehrani and Tsotsos, 2021) or from horizontal connections within the
138 same area (Zhaoping, 2005, Kogo et al., 2010). In V1, feedback and horizontal inputs arrive
139 principally within supragranular and infragranular layers, i.e., they avoid layer 4 (Rockland and
140 Pandya, 1979, Rockland and Lund, 1983, Rockland and Virga, 1989, Anderson and Martin, 2009,
141 Markov et al., 2014, Federer et al., 2021, Gilbert and Wiesel, 1983, Shmuel et al., 2005, Siu et al.,
142 2021). Thus, V1 activity generated by nCRF stimulation is known to involve different circuits
143 compared to the activity generated by CRF stimulation.

In this study, border ownership test stimuli consisted of uniformly white or black objects (squares, 8 x 8 dva) on a black or white background, respectively, as in previous studies (Zhou et al., 2000) (Methods). One border of the object fell within the CRFs of the recorded neurons. Within the CRF, the oriented border could either be a dark-light edge or light-dark edge, resulting in two different local contrast polarity (LC) conditions (Figure 2A). Outside the CRF, the stimulus configuration differed for the same LC condition such that the oriented border could belong to opposite sides of an object relative to the CRF. Crucially, across these two object side conditions, the stimulus falling within the CRF was identical (Figure 2B) and was identical within an area that extended well beyond the CRF (8 x 16, dva). In this stimulus configuration, differences in evoked responses between the two object side conditions signify selectivity to border ownership (Zhou et al., 2000). The statistical significance was determined by a two-factor ANOVA on the mean spike counts for each condition, with object side (Side 1 and Side 2) and local contrast (LC1 and LC2) as the factors, along with their interaction (Methods).

We observed neurons with B_{own} in our recordings from macaque V1. Figures 2C and 2D shows examples of four neurons selective to B_{own}. Each of these neurons exhibited a preference for LC, with two neurons preferring one contrast polarity and two preferring the other. In addition, each neuron responded differently depending on which side of the object appeared relative to the CRF, thus exhibiting B_{own}. Three of the neurons responded more vigorously to borders belonging to the lower-left side of object (Side 1) ($p < 10^{-14}$, 10^{-10}, 10^{-3} for neurons 1, 2, and 4, respectively), while one neuron responded more vigorously to the border belonging to the upper-right side of the

object (Side 2) (p = 0.014, neuron 3). Furthermore, one of the neurons showed a consistent

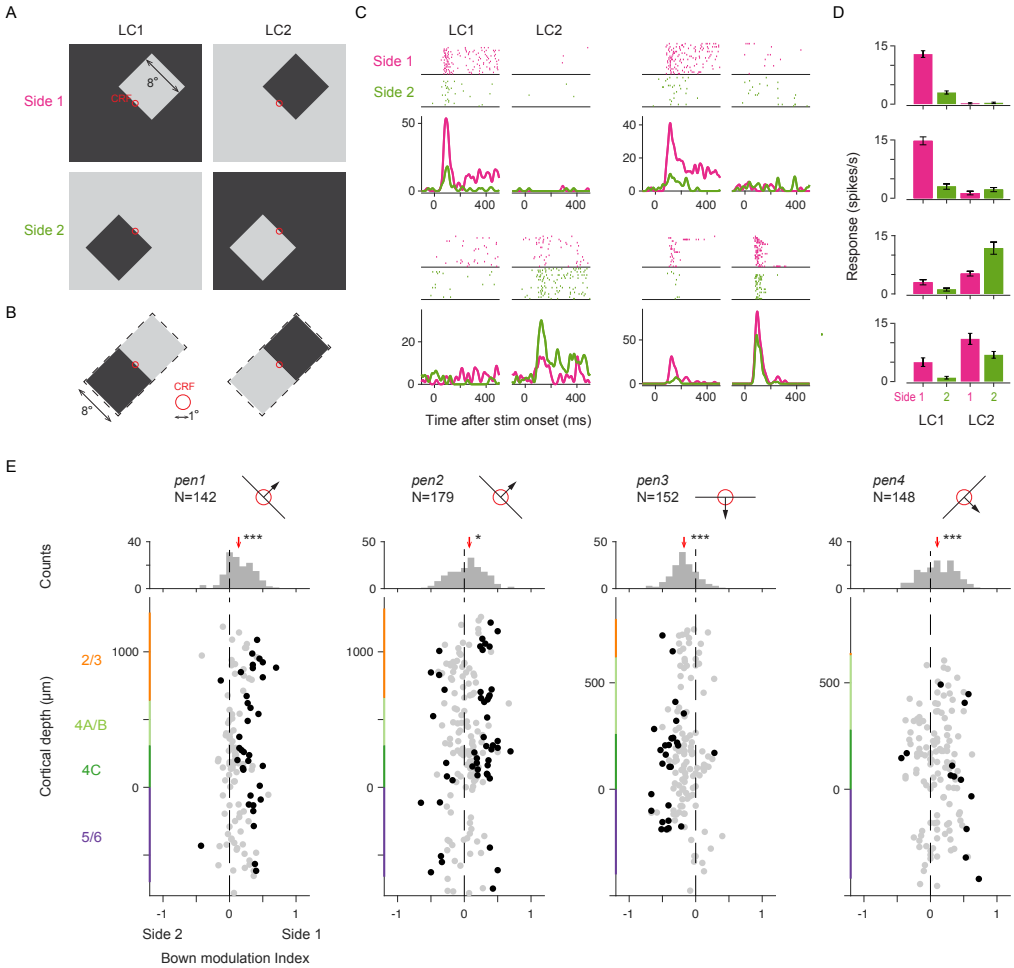

Figure 2. Nonclassical receptive field (nCRF) stimulation and border ownership. (A) Border ownership test stimuli for nCRF stimulation. Stimuli consisted of uniformly white or black objects (8º squares) on black or white backgrounds, respectively. One border of the object fell within the CRFs (red circle) of the recorded neurons, with orientation varying in 45º steps. Within the CRF, depending on local contrast polarity (LC), the border could either be a dark-light edge (LC1, Left column) or a light-dark edge (LC2, Right column). For the same LC condition, the border within the CRF could be the bottom-left edge (Side 1, top row) or top-right edge (Side 2, bottom row) of the object. (B) Enlarged view of stimulus configuration within the CRF, showing identical stimulus regions between Side 1 and Side 2 for each LC condition (8 x 16 dva). (C) Four example B_{own} neurons recorded from V1. For each neuron, dot raster plots (top) and instantaneous firing rates (bottom) show responses to the four stimulus conditions depicted in (A), respectively. Magenta represents Side 1; green represents Side 2. (D) Bar plots showing the mean spike rates of the four neurons across the four stimulus conditions. (E) Top: Cartoon depicting the preferred border orientation for each of the four recording sessions (*pen*1-4). Arrows indicate the preferred side of objects relative to the border in the CRF. Bottom: B_{own} modulation index for each neuron plotted at its recorded cortical depth across the recordings. Color bars on the ordinate represent laminar compartments. Black dots denote statistically significant B_{own} neurons, determined by ANOVA with object side and local contrast as factors ($p < 0.05$). Middle: Marginal distribution of the B_{own} modulation index, red arrows indicating the population median. *$p < 0.05$; ***$p < 10^{-5}$.

165 preference for Side 1 across both LCs (neuron 4).

166 To quantify the B_{own}, as in previous studies (Zhou et al., 2000), we calculated a B_{own}
167 modulation index, defined as the difference in neuronal responses to borders belonging to opposite
168 sides of objects, normalized by the maximum response for each neuron (Methods). Responses to
169 the same side of object, but under opposite LC conditions, were averaged together to control for
170 global luminance differences in the overall display. Across the 621 neurons recorded in four
171 sessions, we found that 133 neurons (21.4% overall; *pen1* = 28.2%; *pen2* = 27.9%; *pen3* = 18.4%;
172 *pen4* = 8.4%) responded differently to identical borders yet belonging to opposite sides of the
173 object, a proportion consistent with previous studies in awake monkeys (Zhou et al., 2000).
174 Neurons with B_{own} were found within all cortical laminar compartments, including input layer 4C
175 (5/6: 28/144 = 19.4%; 4C: 48/212 = 22.6%; 4A/B: 19/114 = 16.7%; 2/3: 28/99 = 28.3%) (Table
176 S1), and the proportion was independent of laminar compartment ($\chi^2(3) = 4.78$, $p = 0.19$, chi-
177 square test of homogeneity). Of all V1 neurons, 96 (15.5%) exhibited B_{own} depending on the LC
178 (5/6: 11.1%; 4C: 17.9%; 4A/B: 14.0%; 2/3: 20.2%), while 37 (6.0%) showed significant effects
179 independent of local contrast (5/6: 8.3%; 4C: 4.7%; 4A/B: 2.6%; 2/3: 8.1%). Thus, the majority of
180 V1 neurons with B_{own} exhibited selectivity for only one local contrast, and neurons with B_{own}
181 invariant to local contrast were rare, also consistent with previous observations (Zhou et al., 2000).
182

183 **Columnar organization of border ownership selectivity**

184 We next considered whether neurons with B_{own} comprised a distinct group, or instead reflected a
185 general tendency of neurons to prefer one side of the object, with statistically significant neurons
186 falling at the tails of the distribution. We leveraged the large number of simultaneously recorded
187 single neurons to measure the distribution of B_{own} modulation across laminar compartments in

188 each session. We found that in each of the four recordings, the distributions of B_{own} modulation
189 generally appeared unimodal, with neurons exhibiting B_{own} falling at the distribution tails (Figure
190 2E). Surprisingly, we also found that within individual recordings, neurons across the cortical
191 depth tended to share similar preferences for the side of the object. That is, for each recording, the
192 B_{own} modulation index differed significantly from 0 (Median modulation index: *pen1* = 0.14, $p <$
193 10^{-12}; *pen2* = 0.08, p = 0.04; *pen3* = -0.18, $p < 10^{-15}$; *pen4* = 0.10, $p < 10^{-5}$, sign test against zero-
194 median). For example, the first recording (*pen1*) was performed in a column in which most neurons
195 preferred an orientation of 135°. In addition, within that column, neurons tended to exhibit higher
196 responses to a border when it belonged to the lower-left side of an object (side 1), as opposed to
197 the upper-right side (side 2). Thus, V1 exhibited a continuum of B_{own}, and neurons within single
198 columns tended to prefer the same side of objects located outside of the CRF.
199

200 **Interlaminar cross-correlations among neurons within single V1 columns**

201 The large number of simultaneously recorded neurons from each session also allowed us to
202 measure interlaminar information flow among single neurons under different visual stimulation
203 conditions. Temporally precise cross-correlations in spike trains offer a unique means of assessing
204 functional interactions among neurons in neural circuits (Perkel et al., 1967). Cross-correlations
205 can be interpreted as suggesting one of myriad putative circuit arrangements among neuronal
206 ensembles (Moore et al., 1970, Aertsen and Gerstein, 1985, Melssen and Epping, 1987, Ostojic et
207 al., 2009). The identification of such interactions has played an important role in elucidating neural
208 circuits in the mammalian visual system (Ts'o et al., 1986, Schwarz and Bolz, 1991, Reid and
209 Alonso, 1995, Alonso et al., 1996, Alonso and Martinez, 1998, Usrey et al., 1998, Nelson et al.,
210 1992, Briggs et al., 2013, Roe and Ts'o, 1999, Senzai et al., 2019, Denman and Contreras, 2014,

211 Siegle et al., 2021, Jia et al., 2022, Trepka et al., 2022, Smith and Kohn, 2008, Sibille et al., 2022).
212 In particular, it has been useful in specifying the flow of signals through local neural circuits
213 (Trepka et al., 2022) and distributed networks (Siegle et al., 2021, Jia et al., 2022, Sibille et al.,
214 2022). Notably, past studies have demonstrated that neuronal cross-correlations are dynamic and
215 can depend on stimulus context and behavioral variables (Hembrook-Short et al., 2019, Martin
216 and von der Heydt, 2015, Hung et al., 2007, Hirabayashi and Miyashita, 2005, Hirabayashi et al.,
217 2010, Steinmetz et al., 2000).

218 Given that V1 activity generated by nCRF stimulation is thought to involve different
219 circuitry than activity generated by CRF stimulation (Angelucci et al., 2017), we next asked if the
220 pattern of cross-correlations measured under classical and nonclassical stimulus conditions might
221 differ in a manner consistent with models of their underlying circuitry. Specifically, modulation
222 of visual responses during nCRF stimulation, such as border ownership stimuli, is thought to
223 emerge from either feedback from higher areas or horizontal connections within the same areas
224 (Bair et al., 2003, Bullier et al., 2001, Hupe et al., 1998, Chen et al., 2017, Gieselmann and Thiele,
225 2022, Keller et al., 2020, Klink et al., 2017, Nassi et al., 2013, Nurminen et al., 2018, Angelucci
226 et al., 2017, Angelucci and Bressloff, 2006, Ichida et al., 2007, Schwabe et al., 2006, Pak et al.,
227 2020, Vangeneugden et al., 2019, Zhang et al., 2014, Adesnik et al., 2012, Chisum et al., 2003,
228 Stettler et al., 2002, Liang et al., 2017, Craft et al., 2007, Jehee et al., 2007, Chen et al., 2014, Self
229 et al., 2013, van Kerkoerle et al., 2014), both arriving principally in superficial and deep layers
230 (Rockland and Lund, 1983, Rockland and Pandya, 1979, Rockland and Virga, 1989, Markov et
231 al., 2014, Federer et al., 2021, Anderson and Martin, 2009, Gilbert and Wiesel, 1983, Shmuel et
232 al., 2005, Siu et al., 2021). In contrast, CRF responses are driven predominantly by feedforward
233 circuitry and geniculocortical inputs to layers 4C and 6 (Hubel and Wiesel, 1972, Hendrickson et

al., 1978, Blasdel and Lund, 1983, Callaway, 1998, Callaway, 2004). This suggests that the pattern of cross-correlations among neurons across V1 layers may differ under CRF and nCRF stimulus conditions.

Across recording sessions, we calculated cross-correlograms (CCGs) from all possible pairwise combinations of neuronal spike trains during both CRF (Gabor gratings) and nCRF (border ownership) stimulation conditions. Figure 3A shows an example recording session (M1, *pen1*) in which 159 visually responsive neurons were recorded during CRF stimulation, and CCGs were computed for 7,956 pairwise combinations of neurons (Methods). CCGs were determined to be significant if the jitter-corrected CCG peak occurred within 10ms of zero-time lag, and exceeded 7 standard deviations (SD) above the mean of the noise distribution (Siegle et al., 2021, Trepka et al., 2022) (Methods). In this recording, 13.8% of the total CCGs computed were found to be significant. Eight significant pairs are highlighted in Figure 3A, with their corresponding CCGs shown in Figure 3B. The peak lag (PL), defined as the relative time delay in occurrence of peak correlation between two spike trains, was restricted to within 10ms. This metric approximates the synchrony and/or the direction of information flow between neuronal pairs (Aertsen and Gerstein, 1985, Moore et al., 1970, Melssen and Epping, 1987, Ostojic et al., 2009). These examples illustrate the tendency of CCGs to corroborate the circuitry within V1 columns under CRF conditions in that 1) PLs generally increase with larger distances between pairs, and 2) layer 4 neurons tend to lead superficial neurons (Trepka et al., 2022). We exploited this latter point to test the extent to which the sequence of information flow across layers differs between CRF and nCRF conditions.

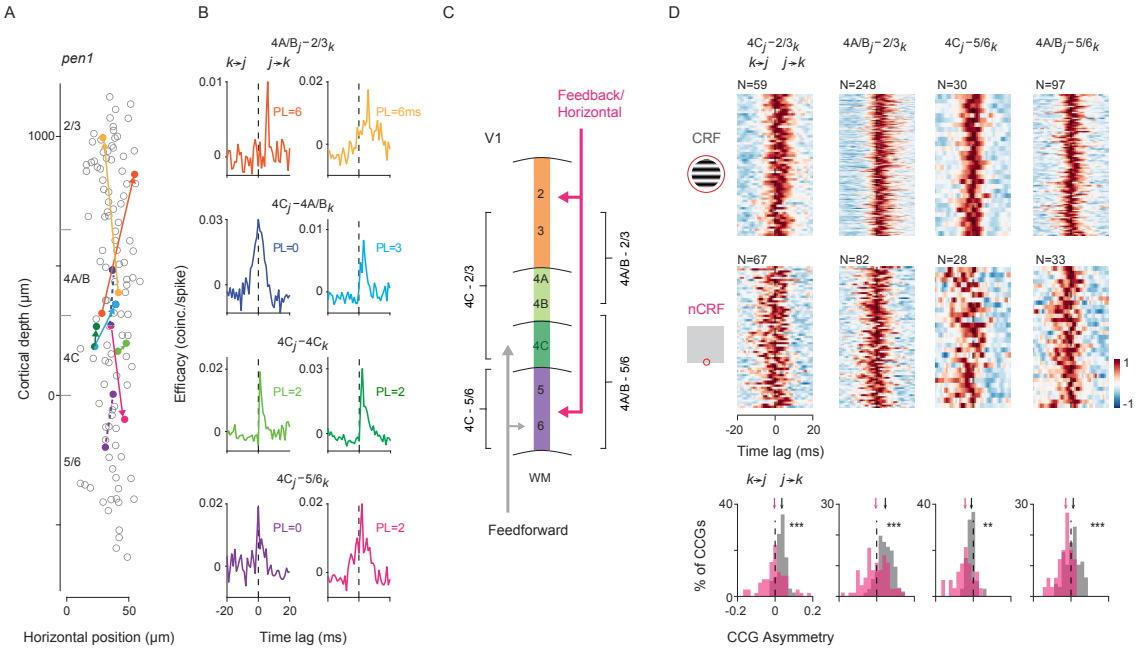

Figure 3. Interlaminar cross-correlations during CRF and nCRF stimulation. (A) Example recording (M1, *pen1*) showing 159 visually responsive neurons (circles) recorded simultaneously during CRF stimulation, plotted at their relative cortical depth. The abscissa is magnified for visualization. Also shown are eight example neuronal pairs with significant CCGs during CRF stimulation. Neuronal pairs with zero-time lag CCGs are connected by dashed lines, while pairs with nonzero-time lag CCGs are connected by arrowed lines, with the arrow pointing to the lagging neuron. (B) Eight corresponding CCGs from (A). Neuronal pairs are separated by their laminar compartment combinations. The reference neuron (1st neuron in the CCG function) is designated as *j*, and the target neuron as *k*. PL (peak lag, ms) is defined as the relative time delay in peak correlation between the two spike trains. (C) Diagram illustrating feedforward and feedback (and horizontal) projections within the designated laminar compartments. Feedforward inputs arrive within laminar compartments 4C and 6, while feedback (and horizontal) projections principally target superficial and deep layers. (D) Heatmap of all significant CCGs during either CRF stimulation (Gabor gratings, top row) or nCRF stimulation (border ownership, middle row), for the four key interlaminar combinations (columns), calculated from one example recording (M1, *pen1*). Individual CCGs are normalized by their absolute maximum for visualization, and different CCGs are vertically stacked. Bottom row: Distribution of CCG asymmetry for each of the four key interlaminar compartments as in (A), across CRF stimulation (gray) and nCRF stimulation (magenta). Arrows indicate the population median. $^{**}p < 0.002$; $^{***}p < 10^{-5}$.

Comparison of cross-correlations during CRF and nCRF stimulation.

From the 677 and 621 neurons recorded across the 4 recording sessions during CRF and nCRF stimulation, there were 41,759 and 28,430 pairwise combinations included, respectively (Methods). Of those, we found that 6,937 (16.6%) and 4,826 (17.0%) of the CCGs were significant

(CRF: *pen1*: 1099/7956 = 13.8%, *pen2*: 2402/11431 = 21.0%, *pen3*: 2174/17780 = 12.2%, *pen4*: 1262/4592 = 27.5%; nCRF: *pen1*: 447/2473 = 18.1%, *pen2*: 2750/11823 = 23.3%, *pen3*: 839/6998 = 12.0%, *pen4*: 790/7136 = 11.1%). Notably, the rates were nearly identical under the two stimulus conditions, and also were within the range observed in previous studies of macaque V1 (Chu et al., 2014, Hembrook-Short et al., 2019, Smith and Kohn, 2008, Kohn and Smith, 2005).

As noted above, modulation of visual responses during nCRF stimulation, such as border ownership stimuli, is thought to be generated principally by feedback/horizontal connections arriving within superficial and deep layers, which contrasts with feedforward input driving CRF stimulation (Figure 3C). Thus, we asked whether cross-correlations between pairs of neurons situated across laminar compartments depended on the type of visual stimulation. We focused our analysis on CCGs computed from pairs of neurons in which one neuron was located within laminar compartments receiving feedback/horizontal inputs (FH_i) and the other was located within compartments largely devoid of those inputs, namely 4C and 4A/B. This analysis compared the relative spike timing between neuronal pairs during CRF and nCRF stimulation. If indeed FH_i contribute more to activity during the latter than the former, then we should expect this to be reflected in lead-lag relationships of the CCGs.

A comparison of V1 CCGs from key interlaminar neuronal pairs during CRF and nCRF stimulation is shown for an example recording session (M1, *pen1*) in Figure 3D. During CRF stimulation, the timing of spikes within compartments 4C and 4A/B generally preceded, or was simultaneous with, spikes within FH_i compartments (CRF: 4C-$2/3_{PL}$ = 2ms, $p < 10^{-7}$; 4A/B-$2/3_{PL}$ = 2ms, $p < 10^{-28}$; 4C-$5/6_{PL}$ = 0ms, p = 0.52; 4A/B-$5/6_{PL}$ = 0ms, p = 0.64; Sign test against zero-median). In contrast, during nCRF stimulation, relative spike timing was shifted in favor of neurons in FH_i compartments. Specifically, during nCRF stimulation, the timing of spikes within

compartments 4C and 4A/B lagged or was simultaneous with, spikes within FH_i compartments (nCRF: 4C-2/3$_{PL}$ = 0ms, p = 0.80; 4A/B-2/3$_{PL}$ = 0ms, p = 0.70; 4C-5/6$_{PL}$ = -2.5ms, p = 0.11; 4A/B-5/6$_{PL}$ = 0ms, p = 0.56; Sign test against zero median). To further quantify the apparent shift in lead-lag relationships, we calculated an asymmetry index for each CCG. The asymmetry index is computed as the difference in the CCG integral on either side of zero-time lag, and summarizes the lead-lag relationship independent of the CCG peak (Jia et al., 2022) (Methods). Consistent with the analyses of PL, we found that CCG asymmetries differed significantly between CRF and nCRF stimulation for each of the interlaminar comparisons. In each case, the distribution of asymmetries during nCRF stimulation shifted to favor neurons in FH_i laminar compartments, when compared to CRF stimulation (4C-2/3: CRF_{Asym} = 0.036, $nCRF_{Asym}$ = -0.004, Δ = -0.04, $p < 10^{-6}$; 4A/B-2/3: CRF_{Asym} = 0.046, $nCRF_{Asym}$ = -0.005, Δ = -0.051, $p < 10^{-11}$; 4C-5/6: CRF_{Asym} = -0.010, $nCRF_{Asym}$ = -0.044, Δ = -0.034, p = 0.0015; 4A/B-5/6: CRF_{Asym} = 0.012, $nCRF_{Asym}$ = -0.028, Δ = -0.04, $p < 10^{-5}$; Wilcoxon rank-sum test). Thus, CCG data from this single recording session indicated that relative spike timing was earlier within FH_i laminar compartments during nCRF stimulation than during CRF stimulation.

Across all recordings, we identified a total of 2,573 and 2,118 significant neuronal pairs from the four interlaminar combinations during CRF (*pen1* = 274; *pen2* = 1187; *pen3* = 560; *pen4* = 302) or nCRF stimulation (*pen1* = 210; *pen2* = 1226; *pen3* = 382; *pen4* = 300), respectively, and compared their CCG asymmetries. Similar to the pattern observed in the example recording, we observed a consistent shift in lead-lag relationships for each of the interlaminar comparisons (Figure 4). Specifically, during nCRF stimulation, the distribution of asymmetries during nCRF stimulation shifted to favor neurons in FH_i laminar compartments, when compared to CRF stimulation (4C-2/3: CRF_{Asym} = 0.028, $nCRF_{Asym}$ = 0.012, Δ = -0.016, $p < 10^{-9}$; 4A/B-2/3: CRF_{Asym}

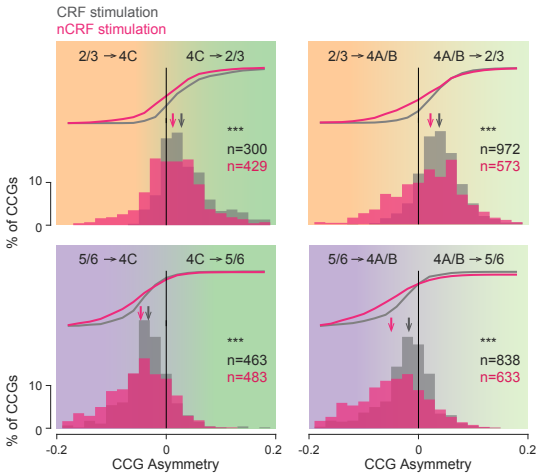

Figure 4. Comparison of interlaminar CCG asymmetries during CRF and nCRF stimulation. Combined dataset for each of the four key interlaminar combinations. Histograms and cumulative distributions of asymmetry for all significant CCGs during CRF (gray) and nCRF (magenta) stimulation. Arrows indicate the population median. ***$p < 10^{-5}$.

= 0.038, $nCRF_{Asym}$ = 0.022, Δ = -0.016, $p < 10^{-9}$; 4C-5/6: CRF_{Asym} = -0.033, $nCRF_{Asym}$ = -0.047, Δ = -0.014, $p < 10^{-5}$; 4A/B-5/6: CRF_{Asym} = -0.018, $nCRF_{Asym}$ = -0.05, Δ = -0.032, $p < 10^{-20}$; Wilcoxon rank-sum test). Thus, relative spike timing was earlier within FH_i laminar compartments during nCRF stimulation than during CRF stimulation in the combined dataset, suggesting that the proportion of information flow from FH_i layers to input layers increased during nCRF stimulation. This observation was consistent across individual recording sessions (Table S2). Notably, we observed a similar pattern when instead of asymmetry, we compared CCG peak lags (Supplementary Figure S2A), and when we compared the total number of both significant and nonsignificant pairs (CRF = 15,920; nCRF = 11,263) (Supplementary Figure S2B), and when we compared CCGs with a more stringent significance criterion (10 SDs) in the combined dataset (Supplementary Figure S2C-D).

Lastly, we asked whether interlaminar information flow was related specifically to border ownership modulation, independent of the comparisons between CRF and nCRF stimulation. Since CRF and nCRF stimuli differed in ways potentially unrelated to nonclassical modulation

319 (e.g., variations within the CRF), we sought to assess the extent to which information flow from
320 FH_i to input layers predicted the magnitude of nCRF modulation. To this end, we computed two
321 modulation indices from the same B_{own} test stimuli (Figure 2A), specifically the B_{own} modulation
322 index and the local contrast (LC) index. In contrast to the B_{own} modulation index, which reflects
323 nCRF modulation, the LC index measures selectivity to luminance contrast polarity (dark-light vs.
324 light-dark) within the CRF. We hypothesized that if the relative timing of spiking activity within
325 FH_i laminar compartments is indicative of nCRF modulation, we should expect earlier relative
326 spike timing in FH_i compartments, i.e., lower CCG asymmetries with respect to other
327 compartments, to be associated with greater B_{own}. In contrast, we should not expect that
328 relationship with the LC index.

329 Consistent with our hypothesis, we observed a negative relationship between the B_{own}
330 modulation index and CCG asymmetry across the population and within individual sessions (linear
331 regression: population slope (β) = -0.32, $p < 10^{-27}$; individual sessions: *pen1* = -0.52, $p < 10^{-5}$; *pen2*
332 = -0.06, p = 0.14; *pen3* = -0.25, $p < 10^{-4}$; *pen4* = -0.20, p = 0.008) (Figure 5A). This result suggests
333 that the magnitude of B_{own} modulation for neuronal pairs depended on the proportion of
334 information flow from FH_i compartment to input layers. In contrast, the opposite was true for the
335 LC index. That is, LC index was positively correlated with CCG asymmetry across the population
336 (linear regression: population slope (β) = 0.46, $p<10^{-28}$) (Figure 5B). However, this relationship
337 was not consistent across sessions (individual sessions: *pen1* = -0.30, p = 0.09; *pen2* = 0.33, p <
338 10^{-5}; *pen3* = 0.23, p = 0.006; *pen4* = 0.14, p = 0.04). To explore both results further, we built
339 generalized linear models (GLMs) to assess the dependence of B_{own} or LC modulation on CCG
340 asymmetry to incorporate variations across interlaminar combinations and recording sessions. For
341 LC modulation, this analysis indicated that the magnitude of LC modulation was not reliably

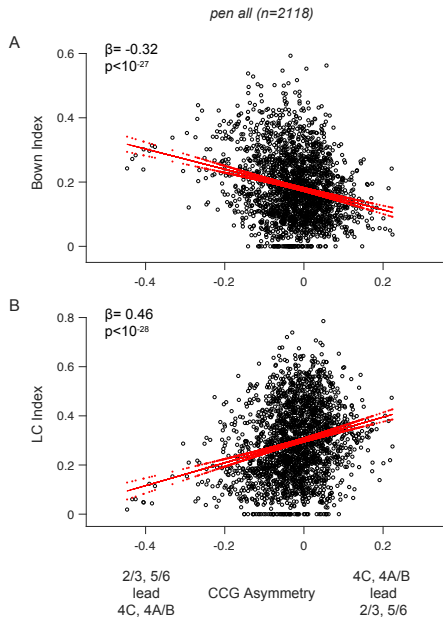

Figure 5. Dependence of nCRF modulation on interlaminar signal flow. (A) Scatter plot of the B_{own} modulation index versus CCG asymmetry for all significant CCGs, aggregated across the four key interlaminar combinations and all recording sessions. CCG asymmetries were calculated during nCRF stimulation. The geometric mean of the B_{own} index for each neuronal pair was used. Red lines denote the fitted regression line and the 95% confidence interval in linear regression. (B) Similar to (A), but using the local contrast (LC) index instead of the B_{own} index. The LC index was calculated as the difference in neuronal responses to borders with opposite contrast polarities, normalized by the maximum response.

predicted by interlaminar information flow (GLM: coefficient = -0.04, p = 0.30; $R^2 = 0.27$) (Table S3). In contrast, for B_{own} modulation, this analysis confirmed that the magnitude of modulation was reliably predicted by interlaminar information flow, independent of variations across interlaminar combinations and recording sessions (GLM: coefficient = -0.16 p = $1.1*10^{-6}$; R^2 = 0.11). These results demonstrate that interlaminar information flow was related specifically to the magnitude of border ownership modulation.

Discussion

We measured the sensitivity of neurons to nCRF stimulation, specifically border ownership, within large, local populations in macaque V1. Consistent with previous studies on awake animals, we observed V1 neurons with border ownership selectivity even under anesthesia. We observed that neurons within single columns tended to prefer the same side of objects located outside of the CRF. In addition, we found that cross-correlations among pairs of neurons situated across FH_i and other laminar compartments differed between CRF and nCRF stimulation. Specifically, neurons within FH_i laminar compartments were more likely to lead pairwise interactions with neurons in other compartments during nCRF stimulation than during CRF stimulation. Moreover, the magnitude of border ownership modulation was predicted by greater information flow from FH_i laminar compartments, independent of the comparisons between CRF and nCRF stimulation. These results demonstrate that the flow of signals between neurons in FH_i and other laminar compartments depends on the degree to which those neurons integrate visual information from beyond the CRF. Below we discuss some potential limitations of the results as well as their implications for the mechanisms underlying contextual modulation.

Each of the laminar compartments designated in this study comprised more than a single distinct anatomical layer. This was done to mitigate the uncertainty in determining exact laminar boundaries, to achieve comparable numbers of neurons across compartments, and to maximize statistical power. In addition, combining layers allowed us to combine feedback with horizontal input layers. It is known that feedback and horizontal connections exhibit layer specificity within superficial and deep layers, e.g., horizontal connections are most prominent in layer 2/3 and layer 5 (Rockland and Lund, 1983, Gilbert and Wiesel, 1983), where feedback connections target primarily in layers 1, upper layer 2, and 5/6 (Rockland and Pandya, 1979, Federer et al., 2021,

371 Shmuel et al., 2005). Yet, they both largely avoid layer 4 (Angelucci et al., 2017). Nonetheless,
372 given that the number of anatomically distinct layers within macaque V1 well exceeds the four
373 designated laminar compartments used here, it is important to consider the extent to which
374 collapsing layers limits the conclusions one can draw from our observations. For example,
375 although layer 6 receives feedback input, it also receives feedforward input directly from the LGN
376 (Hubel and Wiesel, 1972, Hendrickson et al., 1978, Blasdel and Lund, 1983, Callaway, 1998). In
377 addition, layer 4A is generally considered an input layer whereas 4B is not (Callaway, 1998, Hubel
378 and Wiesel, 1972, Blasdel and Lund, 1983, Hendrickson et al., 1978). Thus, the designation of any
379 compartment as nominally input, or feedback was relative and not absolute. That is, superficial
380 and deep layers receive higher proportions of feedback/horizontal inputs than the 4A/B and 4C
381 compartments. Indeed, previous studies of primate visual cortex have used a similar approach in
382 comparing input and feedback/horizontal laminar compartments (e.g. Hansen et al., 2012, Nandy
383 et al., 2017, van Kerkoerle et al., 2017, Pettine et al., 2019). Thus, the observed changes in pattern
384 of cross-correlations between neurons situated across compartments with different relative
385 feedforward and feedback/horizontal input can be interpreted in light of those input differences.

386 Another important consideration is that a key challenge of studying classical and
387 nonclassical RF effects simultaneously in large neuronal populations is the difficulty in achieving
388 alignment of all CRFs with the test stimuli. Although our probe penetrations were largely normal
389 to the surface and neurons showed minimal deviations in orientation selectivity across the cortical
390 depth, V1 neurons nonetheless exhibit noteworthy RF scatter (location/size) even within single
391 cortical columns (Tootell et al., 1988, Gur et al., 2005, Li et al., 2022). This means that the
392 positioning of stimuli relative to the CRF inevitably varied across simultaneously recorded neurons
393 (e.g., Figure 1C). Moreover, this means that although neurons were generally well driven by CRF

394 grating stimuli and exhibited clear orientation tuning, CRF stimulation was not guaranteed to fall
395 solely within the CRF of all neurons. Nonetheless, involvement of the surround, especially far
396 surround was considerably less extensive for CRF stimulation than for nCRF stimulation.
397 Furthermore, in the latter case, regardless of variability in the CRF location, stimuli falling within
398 the CRF were always matched across nCRF stimulus conditions, and the surrounds were also
399 identical within 8° of the CRF (Figure 2A, B).

400 The experiments described here were performed in anesthetized animals. Several other
401 types of contextual modulation have been demonstrated in anesthetized animals (Ramsden et al.,
402 2001, Hupe et al., 1998, Bair et al., 2003, Allman et al., 1985, Gilbert and Wiesel, 1990, Nothdurft
403 et al., 1999, Webb et al., 2003, Zarella and Ts'o, 2016, Muller et al., 2003, Henry et al., 2013,
404 Bijanzadeh et al., 2018), and can involve inter-cortical feedback (Nurminen et al., 2018).
405 Nonetheless, anesthesia is known to affect certain types of contextual responses in area V1. For
406 example, the "figure-ground segregation" effect, where neurons respond more strongly to a texture
407 in a "figure" region than to the same texture in a "ground" region, has been shown to be suppressed
408 under anesthesia (Lamme et al., 1998) and when figure stimuli are not perceived (Super et al.,
409 2001). However, there has been debate over whether this effect depends on attention and awareness
410 (Marcus and Van Essen, 2002, Jones et al., 2015, Poltoratski and Tong, 2020, Poort et al., 2012,
411 Huang et al., 2020). It is worth noting that in that case, RFs are centered on the figure regions, and
412 the modulation likely involves detecting feature discontinuities around boundaries, followed by
413 region-filling and background suppression. Each step could be influenced differently by behavioral
414 variables. Nevertheless, the center figure enhancement emerges late in the V1 response, ~55ms
415 after response onset (Poort et al., 2012). In contrast, border ownership involves RFs centered on
416 the boundaries, with modulation emerging much earlier at ~10-35ms after response onset

417 (Sugihara et al., 2011). Therefore, although both forms of modulation may involve
418 feedback/horizontal input, the underlying circuitry may differ. Our finding of border ownership
419 modulation in anesthetized animals aligns with previous studies showing that border ownership
420 modulation can act separately even without attention (Qiu et al., 2007, O'Herron and von der
421 Heydt, 2009) or before object shape recognition (Williford and von der Heydt, 2016, Ko and von
422 der Heydt, 2018), perhaps signifying a representation of "proto-objects" in the early visual cortex
423 through automatic, pre-attentive grouping mechanism (von der Heydt, 2015, von der Heydt, 2023,
424 Self et al., 2019).

425 Border ownership enables neurons with small CRFs in the early visual cortex to assign the
426 occluding border between image regions to a foreground object, which is crucial for natural scene
427 segmentation and object recognition (Nakayama et al., 1995). Human imaging studies have
428 demonstrated the existence of B_{own} in both lower (Fang et al., 2009) and higher visual areas
429 (Kourtzi and Kanwisher, 2001, Andrews et al., 2002), yet the underlying circuitry is still poorly
430 understood. Several computational models have been proposed to explain B_{own}, including
431 feedforward models (Walker et al., 1999, Sakai and Nishimura, 2006, Super et al., 2010),
432 horizontal models (Zhaoping, 2005, Kogo et al., 2010), and feedback models (Craft et al., 2007,
433 Jehee et al., 2007, Jeurissen et al., 2016). Yet cues for determining B_{own} often lie far from the CRF
434 and beyond the extents of geniculocortical and horizontal V1 connections (Angelucci et al., 2017).
435 Furthermore, conduction along horizontal fibers appears too slow (0.1-0.4 mm/ms) (Grinvald et
436 al., 1994, Bringuier et al., 1999, Girard et al., 2001) to account for the rapid (~10-35ms) emergence
437 of B_{own} and its independence from object size (Zhang and von der Heydt, 2010, Sugihara et al.,
438 2011). In contrast, feedback inputs can be conducted through fibers 10 times faster (20-60 mm/ms)
439 (Girard et al., 2001), even via monosynaptic connections (Siu et al., 2021), and contribute to

modulating the early responses of V1 neurons (Hupe et al., 2001, Bair et al., 2003). Thus, although we combined feedback and horizontal recipient layers, the differences in interlaminar signal flow we observed were likely driven predominantly by feedback inputs.

In primates, V1 receives inter-cortical feedback connections primarily from areas V2, V3, V4, MT (Rockland et al., 1994, Markov et al., 2014). Thus, V1 B_{own} signals could be generated via inputs from these areas (Zhou et al., 2000, Hesse and Tsao, 2016, Hesse and Tsao, 2023, Franken and Reynolds, 2021, Zhu et al., 2020). Our results resonate with a recent study reporting that in area V4, B_{own} emerges earliest in deep layers compared to input layers (Franken and Reynolds, 2021). This suggests that the earliest component of B_{own} in V4 is not inherited from feedforward inputs, i.e., from V1/V2, but is generated within deep layers de nova, or through feedback connections that arrive at deep layers (Franken and Reynolds, 2021). This further supports the view that B_{own} in V1 emerges via feedback from higher visual areas. In addition, similar to what we observed in V1, columnar organization of B_{own} was observed in V4 (Franken and Reynolds, 2021). Indeed, neurons with B_{own} are clustered into patches in a wide range of primate visual areas, including area V2, V3, V3A, V4, V4A (Hesse and Tsao, 2023). Thus, the evidence of B_{own} modularity we observed in V1 could arise from organized feedback from the B_{own} modules in those areas. This is supported by recent anatomical evidence suggesting that feedback terminals in V1 are clustered and functionally specific (Angelucci et al., 2002, Federer et al., 2021, Shmuel et al., 2005, Siu et al., 2021).

459 **Methods**

460 *Experimental Model and Subject Details*

461 Anesthetized recordings were conducted in two adult male rhesus macaques (*Macaca mulatta*,
462 M1, 13 kg; M2, 8 kg). All experimental procedures were in accordance with the National Institutes
463 of Health Guide for the Care and Use of Laboratory Animals, the Society for Neuroscience
464 Guidelines and Policies, and with approved Institutional Animal Care and Use Committee
465 (IACUC) protocol (#APLAC-9900) of Stanford University.

466

467 *Electrophysiological Recordings*

468 Prior to each recording session, treatment with dexamethasone phosphate (2 mg per 24 h) was
469 instituted 24 h to reduce cerebral edema. After administration of ketamine HCl (10 mg per
470 kilogram body weight, intramuscularly), monkeys were ventilated with 1-2% isoflurane in a 1:1
471 mixture of N_2O and O_2 to maintain general anesthesia. Electrocardiogram, respiratory rate, body
472 temperature, blood oxygenation, end-tidal CO_2, urine output and inspired/expired concentrations
473 of anesthetic gasses were monitored continuously. Normal saline was given intravenously at a
474 variable rate to maintain adequate urine output. After a cycloplegic agent (atropine sulfate, 1%)
475 was administered, the eyes were focused with contact lenses on an LCD monitor. Vecuronium
476 bromide (60 μg/kg/h) was infused to prevent eye movements.

477 With the anesthetized monkey in the stereotaxic frame, an occipital craniotomy was
478 performed over the opercular surface of V1. The dura was reflected to expose a small (~3 mm^2)
479 patch of cortex. Next, a region relatively devoid of large surface vessels was selected for
480 implantation, and the Neuropixels probe was inserted with the aid of a surgical microscope. Given
481 the width of the probe (70 μm x 20 μm), insertion of it into the cortex sometimes required multiple

482 attempts if it flexed upon contacting the pia. The junction of the probe tip and the pia could be
483 visualized via the (Zeiss) surgical scope, and the relaxation of pia dimpling was used to indicate
484 penetration, after which the probe was lowered at least 3-4 mm. Prior to probe insertion, it was
485 dipped in a solution of the DiI derivative FM1-43FX (Molecular Probes, Inc) for subsequent
486 histological visualization of the electrode track.

487 Given the length of the probe (1 cm), and the complete distribution of electrode contacts
488 throughout its length, recordings could be made either in the opercular surface cortex (M1, *pen* 1-
489 2) or within the underlying calcarine sulcus (M2, *pen* 3-4), by selecting a subset of contiguous
490 active contacts (n = 384) from the total number (n=986). Recordings were made at 1 to 2 sites in
491 one hemisphere of each monkey. At the end of the experiment, monkeys were euthanized with
492 pentobarbital (150 mg/kg) and perfused with normal saline followed by 1 liter of 1% (wt/vol)
493 paraformaldehyde in 0.1 M phosphate buffer, pH 7.4.

494

495 *Visual Stimulation*

496 Visual stimuli were presented at manually mapped receptive field (RF) locations for each
497 recording session on an LCD monitor (Model NEC-4010, dimensions: 88.5 cm (H) x 49.7 cm (V),
498 resolution: 1360 x 768 pixels, frame rate: 60 Hz) positioned 114 cm from the monkeys. RF
499 eccentricities were ~4-6° (M1) and ~6-10° (M2). Visual stimuli were generated using customized
500 MATLAB scripts with the Psychophysics Toolbox extensions (version PTB-3) (Kleiner et al.,
501 2007). A photodiode was used to measure stimulus timing.

502 Classical receptive field (CRF) stimuli consisted of drifting Gabor gratings (2 deg./sec.,
503 100% Michelson contrast) with a diameter of 1.5 degrees of visual angle (dva), positioned within
504 the joint receptive fields (RFs) of recorded neurons. This size was selected to largely constrain the

505 stimuli within the CRFs of recorded neurons, typically ~0.5-1 dva, as determined manually online.
506 Gratings drifted in 36 different directions, from 0 to 360° in 10° steps, in a pseudorandom order.
507 Each stimulus condition was presented for 1 s and repeated 5 or 10 times. A blank screen with
508 equal luminance to the Gabor patch was presented for 0.25 s during the stimulus interval. Stimuli
509 were presented either monocularly (*pen* 1, 3) or both monocularly and binocularly (*pen* 2, 4). Four
510 spatial frequencies (0.5, 1, 2, 4 cycles/deg.) were tested. The optimal eye and spatial frequency
511 conditions were determined offline for further analysis.

512 Nonclassical receptive field (nCRF) stimuli used in this study, i.e., Border ownership test
513 stimuli consisted of uniformly white or black objects (square, 8 x 8 dva) presented on a black or
514 white background, respectively, like previous studies (Zhou et al., 2000). One border of the object
515 fell within the CRFs of the recorded neurons at an orientation that varied in 45º steps. Objects were
516 either 4 x 4 dva or 8 x 8 dva in size, and only conditions with 8 x 8 dva were selected for quantifying
517 border ownership selectivity to tolerate the variation in the CRF locations. Stimuli were presented
518 monocularly. For each of the 4 orientation conditions, there were 4 basic conditions (Figure 2A).
519 Within the CRF, the oriented border could either be a dark-light edge or light-dark edge, resulting
520 in two different local contrast (LC) polarity conditions, namely, LC1 and LC2. For the same LC
521 condition, the stimulus configuration outside of the CRF differed such that the oriented border
522 could belong opposite sides of objects, resulting in two different sides of object conditions, namely,
523 side 1 and side 2. Each stimulus condition was presented for 1 s and repeated 10 or 20 times. A
524 blank screen with equal luminance to the mean of object and background luminance was presented
525 for 0.5s during the stimulus interval.

526

527 *Receptive field mapping*

528 In some sessions, the receptive fields of V1 neurons were tested systemically for offline use. CRFs
529 were mapped from a 10 x 10 array (4 x 4 dva) using probe stimuli. The array was centered at the
530 manually determined RFs location. The stimuli consisted of circular sine wave gratings of 0.4 dva
531 in diameter, and 100% Michelson contrast. Gratings were presented at the optimal orientation
532 determined manually online for each recording session and drifted at speed of 2 deg./sec. Each
533 stimulus condition was presented for 0.2s, interleaved with 0.3s of blank screen with equal
534 luminance, and repeated 15 times.

535 Mean spike counts from 0.05 to 0.25s after each stimulus onset were calculated, resulting
536 in a 10 x 10 matrix containing mean spike rates to each grid location. This 2D matrix was then
537 interpolated to a 40 x 40 matrix (MATLAB function 'interp2') and then smoothed with a 2D
538 Gaussian filter (MATLAB function 'imgaussfilt', σ=2). The outline of the CRF was defined as the
539 contour isoline at 80% of the maximum response using MATLAB function 'contour3'. Neurons
540 with only 1 contour region at the threshold were selected.

541

542 *Data acquisition and spike sorting*

543 Raw spike-band data were sampled and recorded at 30kHz. They were then median-
544 subtracted and high-pass filtered at 300 Hz during the pre-processing stage. Spike sorting was
545 carried out with Kilosort 3 (Pachitariu et al., 2024) to find spike times and assign each spike to
546 different templates (neurons). Default parameters in Kilosort 3 were used for spike sorting,
547 specifically, Ops.th = [9,9]; Ops.lam = 20; Ops.AUCsplit = 0.8; Ops.ThPre = 8; Ops.sig = 20;
548 Ops.nblocks = 5; Ops.spkTh = -6. The raw sorted data were then manually curated in Phy
549 (*https://github.com/cortex-lab/phy*) to remove templates with very few spikes or with atypical
550 waveforms and to perform minimal templates merging and splitting. Double-counted spikes from

551 the algorithm fitting the residuals to a new template were identified using established criteria
552 (Siegle et al., 2021), by counting spikes from two templates separated by less than 50μm (~5
553 channels) and with spike activity occurring within 5 samples (0.167ms). Double-counted spikes
554 from the template smaller in amplitude were removed from further analysis. Visual responsiveness
555 of each unit was assessed under CRF, nCRF, or RF mapping stimulation. For each type of
556 stimulation, a paired-sample t test was performed to determine whether the mean spike counts after
557 each stimulus presentation exceeded the preceding blank period at a significance level of 0.01.
558 Only neurons showing significant visual responsiveness were included for further analysis.
559
560 *Layer Assignment*
561 The laminar locations of our recorded neurons were estimated based on a combination of
562 functional analysis and histology results. For each recording, we first performed the current source
563 density (CSD) analysis on the stimulus-triggered average of local field potentials (LFP). LFP were
564 low-pass filtered at 200 Hz and recorded at 2500 Hz. LFP signals recorded from every 4 nearby
565 channels were averaged and realigned to the onset of visual stimulus. CSD was estimated as the
566 second-order derivatives of signals along the probe axis using the common five-point formula
567 (Nicholson and Freeman, 1975). The result was then smoothed across space ($\sigma = 120$ μm) to reduce
568 the artifacts caused by varied electrode impedance. We located the lower boundary of the major
569 sink (the reversal point of sink and source) as the border between layer 4C and layer 5/6. We also
570 considered anatomical data in order to localize recorded neurons within gray matter, allowing for
571 minor adjustments (±1 group channel) in layer boundary placement. Subsequent layer boundaries
572 were determined by offsetting the cortical thickness derived from histological slices
573 (Supplementary Fig S1).

574 *Single neuron properties during CRF stimulation*

575 To assess the orientation tuning for each neuron, the spike rates during 0.1 to 1s after each stimulus
576 onset were calculated and averaged for each orientation condition (N= 18). The orientation tuning
577 responses were first smoothed with a Hanning window (half-width at half-height of 20°), and then
578 fitted with a von Mises function (Swindale, 1998)

579 $$y = a_0 + a_1 * e^{a_2*(\cos(2*x-2*a_3)-1)}$$

580 The location of the peak of the fitted curve was determined as the preferred orientation. Only
581 neurons well fit by the function (R^2>0.7) were included for determining pairwise differences in
582 preferences for all combinations in each recording session.

583

584 *Modulation index for border ownership*

585 As in previous studies (Zhou et al., 2000), we calculated a B_{own} modulation index to quantify the
586 selectivity of each neuron for B_{own}. The B_{own} modulation index is defined as

587 $$B_{own}\ index = \frac{0.5 * (R_{LC1} + R_{LC2})_{Side1} - 0.5 * (R_{LC1} + R_{LC2})_{Side2}}{R_{max}}$$

588 Here, $R_{LC,\ Side}$ represents the average spike rate from 0.05 to 0.5 s after stimulus onset for one of
589 four basic conditions, which are derived from the combination of two different *Local Contrast*
590 conditions (LC1 and LC2) and two *Side* conditions (Side 1 and Side 2). Baseline activity was not
591 subtracted. Since the border within the CRF can vary in 45º steps from 0º to 180º, we only selected
592 the optimal orientation for each recording population to calculate the B_{own} index. R_{max} was defined
593 as the maximum response for each neuron across the four basic conditions and four orientations.
594 We used R_{max} instead of summing responses across the four basic conditions to account for the
595 slight variations in orientation preferences among neurons within each recording session. The
596 statistical significance of B_{own} was evaluated using a two-factor ANOVA (MATLAB function

597 ‘anovan’) on the average spike rates for each condition. The two factors were object *Side* (with
598 two levels: Side 1 and Side 2) and *Local Contrast* (with two levels: LC 1 and LC2), including their
599 interactions. A significance level of 0.05 was used. Neurons were considered to exhibit significant
600 B_{own} modulation if they showed a significant main effect for the object *Side* factor. Whether they
601 were invariant to local contrast was determined by the main effect of the *Local Contrast* factor.
602
603 *Cross-correlograms (CCGs)*
604 To measure correlated firing, we computed the cross-correlations between spike trains of
605 all pairs of simultaneously recorded neurons. For each recording session, we calculated cross-
606 correlograms (CCGs) from pairwise combinations of neuronal spike trains during either CRF
607 (Gabor gratings) or nCRF (border ownership) stimulation conditions, respectively. We only
608 included neuronal pairs with geometric mean firing rates more than 0.5 spikes/sec for further
609 analysis. For both conditions, we focused on the spiking activity within the 0.25 -1s window during
610 each stimulus presentation, to mitigate the influence of the transient visual response after stimulus
611 onset. The CCG function for a given pair of neurons was defined as follows:

612 $$CCG(\tau)_{j-k} = \frac{\frac{1}{M}\sum_{i=1}^{M}\sum_{t=1}^{N-\tau} x_j^i\,(t) \times x_k^i(t+\tau)}{\theta(\tau)\sqrt{\lambda_j\lambda_k}}$$

613 where j denotes the first/reference neuron and k denotes the second/target neuron in the CCG
614 function. τ is the time lag between the two spike trains x_j^i and x_k^i from neuron j and k, during trial
615 i. The value of $x_j^i(t)$ and $x_k^i(t)$ is 1 if there is a spike at time bin t and is zero otherwise. M is the
616 total number of trials; N is the number of time bins within a trial. $\theta(\tau) = N - |\tau|$, is a triangular
617 function that corrects for the degree of overlap in the two spike trains at each time lag. λ_j and λ_k
618 are the mean firing rates of neuron j and k computed over the same bins used to compute the CCG

619 at each time lag. The normalization by the geometric mean of spike rates is commonly used by
620 previous studies to account for the influence of firing rates on the CCG peaks (Bair et al., 2001,
621 Kohn and Smith, 2005).

622 To correct for correlations due to stimulus-locking or slow fluctuations in the population
623 responses (e.g., gamma-band activity), we computed a jitter-corrected CCG by subtracting a
624 jittered CCG from the original CCG:

625 $$CCG_{corrected} = CCG_{original} - CCG_{jittered}$$

626 The jittered CCG ($CCG_{jittered}$) reflects the expected value of CCG computed from all possible jitters
627 of each spike train within a given jitter window (Harrison and Geman, 2009, Smith and Kohn,
628 2008). The jittered spike train preserves both the PSTH of the original spike train across trials and
629 the spike counts in the jitter window within each trial. As a result, jitter correction removes the
630 correlation between PSTHs (stimulus-locking) and correlation on timescales longer than the jitter
631 window (slow population correlations). Here, a 25-ms jitter window was chosen based on previous
632 studies (Jia et al., 2013, Siegle et al., 2021). Jitter-corrected CCG ($CCG_{corrected}$) was then smoothed
633 with a 5ms kernel [0.05, 0.25, 0.4, 0.25, 0.05] (Kohn and Smith, 2005, Smith and Kohn, 2008)
634 before further analysis.

635 We classified a CCG as significant if the peak of the jitter-corrected CCG occurred within
636 10 ms of zero and exceeded 7 standard deviations (SD) above the mean of the noise distribution,
637 similar to previous studies (Siegle et al., 2021). The noise distribution for a CCG was defined as
638 the flanks of the jitter-corrected CCG ($\{CCG(\tau)|100 \geq |\tau| \geq 50\ ms\}$). All analyses presented in
639 the main text involve only significant, jitter-corrected CCGs. In the supplementary material, we
640 also applied a more stringent criterion, requiring that significant CCG peaks exceed 10 SD above

641 the noise, and a less stringent criterion that includes both significant and non-significant CCGs.
642 These ensure that our results are robust across the choices of threshold (Supplementary Figure S2).
643 To assess the directionality of functional interactions or signal flow between pairs of
644 neurons, we focused on two metrics derived from the CCG functions. One is the peak lag (PL),
645 which describes the time lag of peak correlation between the spike trains of neuron *k* (target)
646 relative to neuron *j* (reference). PL is positive if the reference neuron *j* leads target neuron *k* in
647 spike timing, negative if *j* lags *k*, and zero if j and k fire synchronously. The second metric we used
648 to assess the signal flow is CCG asymmetry, computed by subtracting the sum of CCG values
649 during the [-13, 0] ms time window from the sum of CCG values during the [0, 13] ms. Similar to
650 PL, a positive CCG asymmetry indicates that reference neuron *j* leads *k*, while a negative
651 asymmetry indicates that *j* lags *k*. The 13ms window was chosen as half of the 25ms jitter window,
652 consistent with previous studies (Jia et al., 2022). Compared to peak lag, CCG asymmetry
653 additionally captures the strength of the functional interactions between pairs of neurons and is
654 less dependent on the exact shape of the CCG peak, which is often more complex in corticocortical
655 functional interactions (Alonso and Martinez, 1998).
656
657 *Relationship between B_{own} modulation and interlaminar signal flow*
658 To determine whether the magnitude of border ownership or local contrast modulation is
659 predicted by interlaminar signal flow during nCRF stimulation, we first performed linear
660 regression (MATLAB, 'fitlm', ordinary least squares) and then built generalized linear models
661 (GLMs) using predictors including CCG asymmetry, interlaminar combinations, and recording
662 sessions. We focused on the four key interlaminar combinations (4C-2/3, 4A/B-2/3, 4C-5/6, 4A/B-
663 5/6), where the latter laminar compartments receive feedback/horizontal inputs (FH_i). Only

neuronal pairs with significant CCGs were included as individual samples in the GLM. The resulting GLM equations were:

$$B_{own}(pair) \sim 1 + asymmetry + \ laminar\ combination + pen$$

$$LC(pair) \sim 1 + asymmetry + \ laminar\ combination + pen$$

B_{own} (pair) and LC (pair) were calculated as the geometric mean of the B_{own} and LC indices for the constituent neurons in each pair. Specifically, $B_{own}(pair) = \sqrt{abs(B_{own}(j)) * abs(B_{own}(k))}$, where abs($B_{own}(j)$) and abs($B_{own}(k)$) represent the absolute B_{own} modulation indices for constituent neurons j and k. A similar calculation was performed for LC (pair). CCG asymmetries were calculated from the nCRF stimulation condition where neurons in the input layers were selected as reference neurons and the ones in FH_i compartments were target neurons in the CCG. Additional predictors, including interlaminar combinations and recording sessions, were included in the models to incorporate variations when pooling the dataset.

Statistical tests

B_{own} for each neuron was assessed with ANOVA. The proportion of B_{own} neurons within different layers was assessed using chi-squared test of homogeneity. The sign of populational border ownership preferences from individual recording session was tested with sign test. The sign of populational CCG peak lag for a given laminar compartment combination was assessed with sign test. The comparisons of peak lag and CCG asymmetry between CRF and nCRF stimulation condition for each laminar compartment combination were evaluated using Wilcoxon rank-sum tests. The dependence between CCG asymmetry and B_{own} for pair of neurons was assessed using linear regression and GLM.

Acknowledgment

We thank Jonathan C. Horton for extensive help with the recordings and histology, Danielle A. Lopes, Stephen Cital, Shellie Hyde and Sam Baker for technical assistance, Tim Harris and Karel Svoboda for providing the Neuropixels probes. This work was supported by NIH Grant EY029759, Brain and Behavior Research Foundation Grant to X.C.; NIH Grants EY014924, NS116623, and a Ben Barres Professorship to T.M.

Author Contributions

Conceptualization, S.Z., X.C. and T.M.; Investigation, S.Z., X.C. and T.M.; Software, S.Z. and E.T.; Formal Analysis, S.Z. and Y.J.O.; Visualization, S.Z., Y.J.O.; Writing – Original Draft, S.Z. and T.M.; Writing – Review and Editing, S.Z., Y.J.O., E.T., X.C., T.M.; Funding Acquisition, X.C. and T.M.

Declaration of Interests

The authors declare no competing interests.

Data and Code Availability

All raw data generated in this study will be deposited in a public repository upon acceptance and made publicly available prior to publication.

The code developed for data analysis has been deposited to GitHub (https://github.com/szhu-007/Zhu_V1_interlaminar-signal-flow) and is freely available for access.

References

ADESNIK, H., BRUNS, W., TANIGUCHI, H., HUANG, Z. J. & SCANZIANI, M. 2012. A neural circuit for spatial summation in visual cortex. *Nature,* 490**,** 226-31.

AERTSEN, A. M. & GERSTEIN, G. L. 1985. Evaluation of neuronal connectivity: sensitivity of cross-correlation. *Brain Res,* 340**,** 341-54.

ALBRIGHT, T. D. & STONER, G. R. 2002. Contextual influences on visual processing. *Annu Rev Neurosci,* 25**,** 339-79.

ALLMAN, J., MIEZIN, F. & MCGUINNESS, E. 1985. Stimulus specific responses from beyond the classical receptive field: neurophysiological mechanisms for local-global comparisons in visual neurons. *Annu Rev Neurosci,* 8**,** 407-30.

ALONSO, J. & CHEN, Y. 2009. Receptive field. *Scholarpedia,* 4**,** 5393.

ALONSO, J. M. & MARTINEZ, L. M. 1998. Functional connectivity between simple cells and complex cells in cat striate cortex. *Nature Neuroscience,* 1**,** 395-403.

ALONSO, J. M., USREY, W. M. & REID, R. C. 1996. Precisely correlated firing in cells of the lateral geniculate nucleus. *Nature,* 383**,** 815-9.

ANDERSON, J. C. & MARTIN, K. A. 2009. The synaptic connections between cortical areas V1 and V2 in macaque monkey. *J Neurosci,* 29**,** 11283-93.

ANDREWS, T. J., SCHLUPPECK, D., HOMFRAY, D., MATTHEWS, P. & BLAKEMORE, C. 2002. Activity in the fusiform gyrus predicts conscious perception of Rubin's vase-face illusion. *Neuroimage,* 17**,** 890-901.

ANGELUCCI, A., BIJANZADEH, M., NURMINEN, L., FEDERER, F., MERLIN, S. & BRESSLOFF, P. C. 2017. Circuits and Mechanisms for Surround Modulation in Visual Cortex. *Annu Rev Neurosci,* 40**,** 425-451.

ANGELUCCI, A. & BRESSLOFF, P. C. 2006. Contribution of feedforward, lateral and feedback connections to the classical receptive field center and extra-classical receptive field surround of primate V1 neurons. *Prog Brain Res,* 154**,** 93-120.

ANGELUCCI, A., LEVITT, J. B., WALTON, E. J., HUPE, J. M., BULLIER, J. & LUND, J. S. 2002. Circuits for local and global signal integration in primary visual cortex. *J Neurosci,* 22**,** 8633-46.

BAIR, W., CAVANAUGH, J. R. & MOVSHON, J. A. 2003. Time course and time-distance relationships for surround suppression in macaque V1 neurons. *J Neurosci,* 23**,** 7690-701.

BAIR, W., ZOHARY, E. & NEWSOME, W. T. 2001. Correlated firing in macaque visual area MT: time scales and relationship to behavior. *J Neurosci,* 21**,** 1676-97.

BIJANZADEH, M., NURMINEN, L., MERLIN, S., CLARK, A. M. & ANGELUCCI, A. 2018. Distinct Laminar Processing of Local and Global Context in Primate Primary Visual Cortex. *Neuron,* 100**,** 259-274 e4.

BLASDEL, G. G. & LUND, J. S. 1983. Termination of afferent axons in macaque striate cortex. *J Neurosci,* 3**,** 1389-413.

BRIGGS, F., MANGUN, G. R. & USREY, W. M. 2013. Attention enhances synaptic efficacy and the signal-to-noise ratio in neural circuits. *Nature,* 499**,** 476-80.

BRINGUIER, V., CHAVANE, F., GLAESER, L. & FREGNAC, Y. 1999. Horizontal propagation of visual activity in the synaptic integration field of area 17 neurons. *Science,* 283**,** 695-9.

BULLIER, J., HUPE, J. M., JAMES, A. C. & GIRARD, P. 2001. The role of feedback connections in shaping the responses of visual cortical neurons. *Prog Brain Res,* 134**,** 193-204.

CALLAWAY, E. M. 1998. Local circuits in primary visual cortex of the macaque monkey. *Annu Rev Neurosci,* 21**,** 47-74.

CALLAWAY, E. M. 2004. Feedforward, feedback and inhibitory connections in primate visual cortex. *Neural Netw,* 17**,** 625-32.

CHEN, M., YAN, Y., GONG, X., GILBERT, C. D., LIANG, H. & LI, W. 2014. Incremental integration of global contours through interplay between visual cortical areas. *Neuron,* 82**,** 682-94.

CHEN, R., WANG, F., LIANG, H. & LI, W. 2017. Synergistic Processing of Visual Contours across Cortical Layers in V1 and V2. *Neuron,* 96**,** 1388-1402 e4.
CHISUM, H. J., MOOSER, F. & FITZPATRICK, D. 2003. Emergent properties of layer 2/3 neurons reflect the collinear arrangement of horizontal connections in tree shrew visual cortex. *J Neurosci,* 23**,** 2947-60.
CHU, C. C., CHIEN, P. F. & HUNG, C. P. 2014. Tuning dissimilarity explains short distance decline of spontaneous spike correlation in macaque V1. *Vision Res,* 96**,** 113-32.
CRAFT, E., SCHÜTZE, H., NIEBUR, E. & VON DER HEYDT, R. 2007. A neural model of figure-ground organization. *J. Neurophysiol,* 97**,** 4310-4326.
DENMAN, D. J. & CONTRERAS, D. 2014. The structure of pairwise correlation in mouse primary visual cortex reveals functional organization in the absence of an orientation map. *Cereb Cortex,* 24**,** 2707-20.
EGUCHI, A. & STRINGER, S. M. 2016. Neural network model develops border ownership representation through visually guided learning. *Neurobiol Learn Mem,* 136**,** 147-165.
FANG, F., BOYACI, H. & KERSTEN, D. 2009. Border ownership selectivity in human early visual cortex and its modulation by attention. *J Neurosci,* 29**,** 460-5.
FEDERER, F., TA'AFUA, S., MERLIN, S., HASSANPOUR, M. S. & ANGELUCCI, A. 2021. Stream-specific feedback inputs to the primate primary visual cortex. *Nat Commun,* 12**,** 228.
FITZPATRICK, D. 2000. Seeing beyond the receptive field in primary visual cortex. *Curr Opin Neurobiol,* 10**,** 438-43.
FRANKEN, T. P. & REYNOLDS, J. H. 2021. Columnar processing of border ownership in primate visual cortex. *Elife,* 10.
GIESELMANN, M. A. & THIELE, A. 2022. Stimulus dependence of directed information exchange between cortical layers in macaque V1. *Elife,* 11.
GILBERT, C. D. & WIESEL, T. N. 1983. Clustered intrinsic connections in cat visual cortex. *J Neurosci,* 3**,** 1116-33.
GILBERT, C. D. & WIESEL, T. N. 1990. The influence of contextual stimuli on the orientation selectivity of cells in primary visual cortex of the cat. *Vision Res,* 30**,** 1689-701.
GIRARD, P., HUPE, J. M. & BULLIER, J. 2001. Feedforward and feedback connections between areas V1 and V2 of the monkey have similar rapid conduction velocities. *J Neurophysiol,* 85**,** 1328-31.
GRINVALD, A., LIEKE, E. E., FROSTIG, R. D. & HILDESHEIM, R. 1994. Cortical point-spread function and long-range lateral interactions revealed by real-time optical imaging of macaque monkey primary visual cortex. *J Neurosci,* 14**,** 2545-68.
GUR, M., KAGAN, I. & SNODDERLY, D. M. 2005. Orientation and direction selectivity of neurons in V1 of alert monkeys: functional relationships and laminar distributions. *Cereb Cortex,* 15**,** 1207-21.
HANSEN, B. J., CHELARU, M. I. & DRAGOI, V. 2012. Correlated variability in laminar cortical circuits. *Neuron,* 76**,** 590-602.
HARRISON, M. T. & GEMAN, S. 2009. A rate and history-preserving resampling algorithm for neural spike trains. *Neural Comput,* 21**,** 1244-58.
HARTLINE, H. K. 1938. THE RESPONSE OF SINGLE OPTIC NERVE FIBERS OF THE VERTEBRATE EYE TO ILLUMINATION OF THE RETINA. *American Journal of Physiology-Legacy Content,* 121**,** 400-415.
HEMBROOK-SHORT, J. R., MOCK, V. L., USREY, W. M. & BRIGGS, F. 2019. Attention Enhances the Efficacy of Communication in V1 Local Circuits. *J Neurosci,* 39**,** 1066-1076.
HENDRICKSON, A. E., WILSON, J. R. & OGREN, M. P. 1978. The neuroanatomical organization of pathways between the dorsal lateral geniculate nucleus and visual cortex in Old World and New World primates. *J Comp Neurol,* 182**,** 123-36.
HENRY, C. A., JOSHI, S., XING, D., SHAPLEY, R. M. & HAWKEN, M. J. 2013. Functional characterization of the extraclassical receptive field in macaque V1: contrast, orientation, and temporal dynamics. *J Neurosci,* 33**,** 6230-42.
HESSE, J. K. & TSAO, D. Y. 2016. Consistency of Border-Ownership Cells across Artificial Stimuli, Natural Stimuli, and Stimuli with Ambiguous Contours. *J Neurosci,* 36**,** 11338-11349.

HESSE, J. K. & TSAO, D. Y. 2023. Functional modules for visual scene segmentation in macaque visual cortex. *Proc Natl Acad Sci U S A,* 120**,** e2221122120.

HIRABAYASHI, T. & MIYASHITA, Y. 2005. Dynamically modulated spike correlation in monkey inferior temporal cortex depending on the feature configuration within a whole object. *J Neurosci,* 25**,** 10299-307.

HIRABAYASHI, T., TAKEUCHI, D., TAMURA, K. & MIYASHITA, Y. 2010. Triphasic dynamics of stimulus-dependent information flow between single neurons in macaque inferior temporal cortex. *J Neurosci,* 30**,** 10407-21.

HUANG, L., WANG, L., SHEN, W., LI, M., WANG, S., WANG, X., UNGERLEIDER, L. G. & ZHANG, X. 2020. A source for awareness-dependent figure-ground segregation in human prefrontal cortex. *Proc Natl Acad Sci U S A,* 117**,** 30836-30847.

HUBEL, D. H. & WIESEL, T. N. 1972. Laminar and columnar distribution of geniculo-cortical fibers in the macaque monkey. *J Comp Neurol,* 146**,** 421-50.

HUNG, C. P., RAMSDEN, B. M. & ROE, A. W. 2007. A functional circuitry for edge-induced brightness perception. *Nat Neurosci,* 10**,** 1185-90.

HUPE, J. M., JAMES, A. C., GIRARD, P., LOMBER, S. G., PAYNE, B. R. & BULLIER, J. 2001. Feedback connections act on the early part of the responses in monkey visual cortex. *J Neurophysiol,* 85**,** 134-45.

HUPE, J. M., JAMES, A. C., PAYNE, B. R., LOMBER, S. G., GIRARD, P. & BULLIER, J. 1998. Cortical feedback improves discrimination between figure and background by V1, V2 and V3 neurons. *Nature,* 394**,** 784-7.

ICHIDA, J. M., SCHWABE, L., BRESSLOFF, P. C. & ANGELUCCI, A. 2007. Response facilitation from the "suppressive" receptive field surround of macaque V1 neurons. *J Neurophysiol,* 98**,** 2168-81.

JEHEE, J. F., LAMME, V. A. & ROELFSEMA, P. R. 2007. Boundary assignment in a recurrent network architecture. *Vision Res,* 47**,** 1153-65.

JEURISSEN, D., SELF, M. W. & ROELFSEMA, P. R. 2016. Serial grouping of 2D-image regions with object-based attention in humans. *Elife,* 5.

JIA, X., TANABE, S. & KOHN, A. 2013. gamma and the coordination of spiking activity in early visual cortex. *Neuron,* 77**,** 762-74.

JIA, X. X., SIEGLE, J. H., DURAND, S., HELLER, G., RAMIREZ, T. K., KOCH, C. & OLSEN, S. R. 2022. Multi-regional module-based signal transmission in mouse visual cortex. *Neuron,* 110**,** 1585-+.

JONES, H. E., ANDOLINA, I. M., SHIPP, S. D., ADAMS, D. L., CUDEIRO, J., SALT, T. E. & SILLITO, A. M. 2015. Figure-ground modulation in awake primate thalamus. *Proc Natl Acad Sci U S A,* 112**,** 7085-90.

JUN, J. J., STEINMETZ, N. A., SIEGLE, J. H., DENMAN, D. J., BAUZA, M., BARBARITS, B., LEE, A. K., ANASTASSIOU, C. A., ANDREI, A., AYDIN, C., BARBIC, M., BLANCHE, T. J., BONIN, V., COUTO, J., DUTTA, B., GRATIY, S. L., GUTNISKY, D. A., HAUSSER, M., KARSH, B., LEDOCHOWITSCH, P., LOPEZ, C. M., MITELUT, C., MUSA, S., OKUN, M., PACHITARIU, M., PUTZEYS, J., RICH, P. D., ROSSANT, C., SUN, W. L., SVOBODA, K., CARANDINI, M., HARRIS, K. D., KOCH, C., O'KEEFE, J. & HARRIS, T. D. 2017. Fully integrated silicon probes for high-density recording of neural activity. *Nature,* 551**,** 232-236.

KAPADIA, M. K., ITO, M., GILBERT, C. D. & WESTHEIMER, G. 1995. Improvement in visual sensitivity by changes in local context: parallel studies in human observers and in V1 of alert monkeys. *Neuron,* 15**,** 843-56.

KELLER, A. J., ROTH, M. M. & SCANZIANI, M. 2020. Feedback generates a second receptive field in neurons of the visual cortex. *Nature,* 582**,** 545-549.

KLEINER, M., BRAINARD, D. & PELLI, D. 2007. What's new in Psychtoolbox-3? *Perception,* 36**,** 14-14.

KLINK, P. C., DAGNINO, B., GARIEL-MATHIS, M. A. & ROELFSEMA, P. R. 2017. Distinct Feedforward and Feedback Effects of Microstimulation in Visual Cortex Reveal Neural Mechanisms of Texture Segregation. *Neuron,* 95**,** 209-220 e3.

KNIERIM, J. J. & VAN ESSEN, D. C. 1992. Neuronal responses to static texture patterns in area V1 of the alert macaque monkey. *J Neurophysiol,* 67**,** 961-80.
KO, H. K. & VON DER HEYDT, R. 2018. Figure-ground organization in the visual cortex: does meaning matter? *J Neurophysiol,* 119**,** 160-176.
KOGO, N., STRECHA, C., VAN GOOL, L. & WAGEMANS, J. 2010. Surface construction by a 2-D differentiation-integration process: a neurocomputational model for perceived border ownership, depth, and lightness in Kanizsa figures. *Psychol Rev,* 117**,** 406-39.
KOHN, A. & SMITH, M. A. 2005. Stimulus dependence of neuronal correlation in primary visual cortex of the macaque. *J Neurosci,* 25**,** 3661-73.
KOURTZI, Z. & KANWISHER, N. 2001. Representation of perceived object shape by the human lateral occipital complex. *Science,* 293**,** 1506-9.
LAMME, V. A. 1995. The neurophysiology of figure-ground segregation in primary visual cortex. *J Neurosci,* 15**,** 1605-15.
LAMME, V. A., ZIPSER, K. & SPEKREIJSE, H. 1998. Figure-ground activity in primary visual cortex is suppressed by anesthesia. *Proc Natl Acad Sci U S A,* 95**,** 3263-8.
LAYTON, O. W., MINGOLLA, E. & YAZDANBAKHSH, A. 2012. Dynamic coding of border-ownership in visual cortex. *J Vis,* 12**,** 8.
LEE, T. S., YANG, C. F., ROMERO, R. D. & MUMFORD, D. 2002. Neural activity in early visual cortex reflects behavioral experience and higher-order perceptual saliency. *Nat Neurosci,* 5**,** 589-97.
LI, W., PIECH, V. & GILBERT, C. D. 2006. Contour saliency in primary visual cortex. *Neuron,* 50**,** 951-62.
LI, Y., WANG, T., YANG, Y., DAI, W., WU, Y., LI, L., HAN, C., ZHONG, L., LI, L., WANG, G., DOU, F. & XING, D. 2022. Cascaded normalizations for spatial integration in the primary visual cortex of primates. *Cell Rep,* 40**,** 111221.
LIANG, H., GONG, X., CHEN, M., YAN, Y., LI, W. & GILBERT, C. D. 2017. Interactions between feedback and lateral connections in the primary visual cortex. *Proc Natl Acad Sci U S A,* 114**,** 8637-8642.
LUND, J. S. 1973. Organization of neurons in the visual cortex, area 17, of the monkey (Macaca mulatta). *J Comp Neurol,* 147**,** 455-96.
MARCUS, D. S. & VAN ESSEN, D. C. 2002. Scene segmentation and attention in primate cortical areas V1 and V2. *J Neurophysiol,* 88**,** 2648-58.
MARKOV, N. T., VEZOLI, J., CHAMEAU, P., FALCHIER, A., QUILODRAN, R., HUISSOUD, C., LAMY, C., MISERY, P., GIROUD, P., ULLMAN, S., BARONE, P., DEHAY, C., KNOBLAUCH, K. & KENNEDY, H. 2014. Anatomy of hierarchy: feedforward and feedback pathways in macaque visual cortex. *J Comp Neurol,* 522**,** 225-59.
MARTIN, A. B. & VON DER HEYDT, R. 2015. Spike synchrony reveals emergence of proto-objects in visual cortex. *Journal of Neuroscience,* 35**,** 6860-6870.
MEHRANI, P. & TSOTSOS, J. K. 2021. Early recurrence enables figure border ownership. *Vision Res,* 186**,** 23-33.
MELSSEN, W. J. & EPPING, W. J. 1987. Detection and estimation of neural connectivity based on crosscorrelation analysis. *Biol Cybern,* 57**,** 403-14.
MOORE, G. P., SEGUNDO, J. P., PERKEL, D. H. & LEVITAN, H. 1970. Statistical signs of synaptic interaction in neurons. *Biophys J,* 10**,** 876-900.
MULLER, J. R., METHA, A. B., KRAUSKOPF, J. & LENNIE, P. 2003. Local signals from beyond the receptive fields of striate cortical neurons. *J Neurophysiol,* 90**,** 822-31.
NAKAYAMA, K., HE, Z. J. & SHIMOJO, S. 1995. Visual Surface Representation: A Critical Link between Lower-Level and Higher-Level Vision. *In:* KOSSLYN, S. M. & OSHERSON, D. N. (eds.) *An Invitation to Cognitive Science, Volume 2: Visual Cognition.* The MIT Press.
NANDY, A. S., NASSI, J. J. & REYNOLDS, J. H. 2017. Laminar Organization of Attentional Modulation in Macaque Visual Area V4. *Neuron,* 93**,** 235-246.
NASSI, J. J., LOMBER, S. G. & BORN, R. T. 2013. Corticocortical feedback contributes to surround suppression in V1 of the alert primate. *J Neurosci,* 33**,** 8504-17.

NELSON, J. I. & FROST, B. J. 1985. Intracortical facilitation among co-oriented, co-axially aligned simple cells in cat striate cortex. *Exp Brain Res,* 61**,** 54-61.
NELSON, J. I., SALIN, P. A., MUNK, M. H., ARZI, M. & BULLIER, J. 1992. Spatial and temporal coherence in cortico-cortical connections: a cross-correlation study in areas 17 and 18 in the cat. *Vis Neurosci,* 9**,** 21-37.
NICHOLSON, C. & FREEMAN, J. A. 1975. Theory of current source-density analysis and determination of conductivity tensor for anuran cerebellum. *J Neurophysiol,* 38**,** 356-68.
NOTHDURFT, H. C., GALLANT, J. L. & VAN ESSEN, D. C. 1999. Response modulation by texture surround in primate area V1: correlates of "popout" under anesthesia. *Vis Neurosci,* 16**,** 15-34.
NURMINEN, L., MERLIN, S., BIJANZADEH, M., FEDERER, F. & ANGELUCCI, A. 2018. Top-down feedback controls spatial summation and response amplitude in primate visual cortex. *Nat Commun,* 9**,** 2281.
O'HERRON, P. J. & VON DER HEYDT, R. 2009. Short-term memory for figure-ground organization in the visual cortex. *Neuron,* 61**,** 801-809.
O'KUSKY, J. & COLONNIER, M. 1982. A laminar analysis of the number of neurons, glia, and synapses in the adult cortex (area 17) of adult macaque monkeys. *J Comp Neurol,* 210**,** 278-90.
OSTOJIC, S., BRUNEL, N. & HAKIM, V. 2009. How connectivity, background activity, and synaptic properties shape the cross-correlation between spike trains. *J Neurosci,* 29**,** 10234-53.
PACHITARIU, M., SRIDHAR, S., PENNINGTON, J. & STRINGER, C. 2024. Spike sorting with Kilosort4. *Nat Methods,* 21**,** 914-921.
PAK, A., RYU, E., LI, C. & CHUBYKIN, A. A. 2020. Top-Down Feedback Controls the Cortical Representation of Illusory Contours in Mouse Primary Visual Cortex. *J Neurosci,* 40**,** 648-660.
PERKEL, D. H., GERSTEIN, G. L. & MOORE, G. P. 1967. Neuronal spike trains and stochastic point processes. II. Simultaneous spike trains. *Biophys J,* 7**,** 419-40.
PETTINE, W. W., STEINMETZ, N. A. & MOORE, T. 2019. Laminar segregation of sensory coding and behavioral readout in macaque V4. *Proc Natl Acad Sci U S A,* 116**,** 14749-14754.
POLTORATSKI, S. & TONG, F. 2020. Resolving the Spatial Profile of Figure Enhancement in Human V1 through Population Receptive Field Modeling. *J Neurosci,* 40**,** 3292-3303.
POORT, J., RAUDIES, F., WANNIG, A., LAMME, V. A., NEUMANN, H. & ROELFSEMA, P. R. 2012. The role of attention in figure-ground segregation in areas V1 and V4 of the visual cortex. *Neuron,* 75**,** 143-56.
QIU, F. T., SUGIHARA, T. & VON DER HEYDT, R. 2007. Figure-ground mechanisms provide structure for selective attention. *Nature Neuroscience,* 10**,** 1492-1499.
RAMSDEN, B. M., HUNG, C. P. & ROE, A. W. 2001. Real and illusory contour processing in area V1 of the primate: a cortical balancing act. *Cereb Cortex,* 11**,** 648-65.
REID, R. C. & ALONSO, J. M. 1995. Specificity of monosynaptic connections from thalamus to visual cortex. *Nature,* 378**,** 281-4.
ROCKLAND, K. S. & LUND, J. S. 1983. Intrinsic laminar lattice connections in primate visual cortex. *J Comp Neurol,* 216**,** 303-18.
ROCKLAND, K. S. & PANDYA, D. N. 1979. Laminar origins and terminations of cortical connections of the occipital lobe in the rhesus monkey. *Brain Res,* 179**,** 3-20.
ROCKLAND, K. S., SALEEM, K. S. & TANAKA, K. 1994. Divergent feedback connections from areas V4 and TEO in the macaque. *Vis Neurosci,* 11**,** 579-600.
ROCKLAND, K. S. & VIRGA, A. 1989. Terminal arbors of individual "feedback" axons projecting from area V2 to V1 in the macaque monkey: a study using immunohistochemistry of anterogradely transported Phaseolus vulgaris-leucoagglutinin. *J Comp Neurol,* 285**,** 54-72.
ROE, A. W. & TS'O, D. Y. 1999. Specificity of color connectivity between primate V1 and V2. *J Neurophysiol,* 82**,** 2719-30.
ROELFSEMA, P. R. 2006. Cortical algorithms for perceptual grouping. *Annu Rev Neurosci,* 29**,** 203-27.
SAKAI, K. & NISHIMURA, H. 2006. Surrounding suppression and facilitation in the determination of border ownership. *J Cogn Neurosci,* 18**,** 562-79.

SCHWABE, L., OBERMAYER, K., ANGELUCCI, A. & BRESSLOFF, P. C. 2006. The role of feedback in shaping the extra-classical receptive field of cortical neurons: a recurrent network model. *J Neurosci,* 26**,** 9117-29.

SCHWARZ, C. & BOLZ, J. 1991. Functional specificity of a long-range horizontal connection in cat visual cortex: a cross-correlation study. *J Neurosci,* 11**,** 2995-3007.

SELF, M. W., JEURISSEN, D., VAN HAM, A. F., VAN VUGT, B., POORT, J. & ROELFSEMA, P. R. 2019. The Segmentation of Proto-Objects in the Monkey Primary Visual Cortex. *Curr Biol,* 29**,** 1019-1029 e4.

SELF, M. W., VAN KERKOERLE, T., SUPER, H. & ROELFSEMA, P. R. 2013. Distinct roles of the cortical layers of area V1 in figure-ground segregation. *Curr Biol,* 23**,** 2121-9.

SENZAI, Y., FERNANDEZ-RUIZ, A. & BUZSAKI, G. 2019. Layer-Specific Physiological Features and Interlaminar Interactions in the Primary Visual Cortex of the Mouse. *Neuron,* 101**,** 500-513 e5.

SHMUEL, A., KORMAN, M., STERKIN, A., HAREL, M., ULLMAN, S., MALACH, R. & GRINVALD, A. 2005. Retinotopic axis specificity and selective clustering of feedback projections from V2 to V1 in the owl monkey. *J Neurosci,* 25**,** 2117-31.

SIBILLE, J., GEHR, C., BENICHOV, J. I., BALASUBRAMANIAN, H., TEH, K. L., LUPASHINA, T., VALLENTIN, D. & KREMKOW, J. 2022. High-density electrode recordings reveal strong and specific connections between retinal ganglion cells and midbrain neurons. *Nature Communications,* 13.

SIEGLE, J. H., JIA, X., DURAND, S., GALE, S., BENNETT, C., GRADDIS, N., HELLER, G., RAMIREZ, T. K., CHOI, H., LUVIANO, J. A., GROBLEWSKI, P. A., AHMED, R., ARKHIPOV, A., BERNARD, A., BILLEH, Y. N., BROWN, D., BUICE, M. A., CAIN, N., CALDEJON, S., CASAL, L., CHO, A., CHVILICEK, M., COX, T. C., DAI, K., DENMAN, D. J., DE VRIES, S. E. J., DIETZMAN, R., ESPOSITO, L., FARRELL, C., FENG, D., GALBRAITH, J., GARRETT, M., GELFAND, E. C., HANCOCK, N., HARRIS, J. A., HOWARD, R., HU, B., HYTNEN, R., IYER, R., JESSETT, E., JOHNSON, K., KATO, I., KIGGINS, J., LAMBERT, S., LECOQ, J., LEDOCHOWITSCH, P., LEE, J. H., LEON, A., LI, Y., LIANG, E., LONG, F., MACE, K., MELCHIOR, J., MILLMAN, D., MOLLENKOPF, T., NAYAN, C., NG, L., NGO, K., NGUYEN, T., NICOVICH, P. R., NORTH, K., OCKER, G. K., OLLERENSHAW, D., OLIVER, M., PACHITARIU, M., PERKINS, J., REDING, M., REID, D., ROBERTSON, M., RONELLENFITCH, K., SEID, S., SLAUGHTERBECK, C., STOECKLIN, M., SULLIVAN, D., SUTTON, B., SWAPP, J., THOMPSON, C., TURNER, K., WAKEMAN, W., WHITESELL, J. D., WILLIAMS, D., WILLIFORD, A., YOUNG, R., ZENG, H., NAYLOR, S., PHILLIPS, J. W., REID, R. C., MIHALAS, S., OLSEN, S. R. & KOCH, C. 2021. Survey of spiking in the mouse visual system reveals functional hierarchy. *Nature,* 592**,** 86-92.

SILLITO, A. M., GRIEVE, K. L., JONES, H. E., CUDEIRO, J. & DAVIS, J. 1995. Visual cortical mechanisms detecting focal orientation discontinuities. *Nature,* 378**,** 492-6.

SIU, C., BALSOR, J., MERLIN, S., FEDERER, F. & ANGELUCCI, A. 2021. A direct interareal feedback-to-feedforward circuit in primate visual cortex. *Nat Commun,* 12**,** 4911.

SMITH, M. A. & KOHN, A. 2008. Spatial and temporal scales of neuronal correlation in primary visual cortex. *J Neurosci,* 28**,** 12591-603.

STEINMETZ, P. N., ROY, A., FITZGERALD, P. J., HSIAO, S. S., JOHNSON, K. O. & NIEBUR, E. 2000. Attention modulates synchronized neuronal firing in primate somatosensory cortex. *Nature,* 404**,** 187-90.

STETTLER, D. D., DAS, A., BENNETT, J. & GILBERT, C. D. 2002. Lateral connectivity and contextual interactions in macaque primary visual cortex. *Neuron,* 36**,** 739-50.

SUGIHARA, T., QIU, F. T. & VON DER HEYDT, R. 2011. The speed of context integration in the visual cortex. *J Neurophysiol,* 106**,** 374-85.

SUPER, H., ROMEO, A. & KEIL, M. 2010. Feed-forward segmentation of figure-ground and assignment of border-ownership. *PLoS One,* 5**,** e10705.

SUPER, H., SPEKREIJSE, H. & LAMME, V. A. 2001. Two distinct modes of sensory processing observed in monkey primary visual cortex (V1). *Nat Neurosci,* 4**,** 304-10.

SWINDALE, N. V. 1998. Orientation tuning curves: empirical description and estimation of parameters. *Biol Cybern,* 78**,** 45-56.
TOOTELL, R. B., SWITKES, E., SILVERMAN, M. S. & HAMILTON, S. L. 1988. Functional anatomy of macaque striate cortex. II. Retinotopic organization. *J Neurosci,* 8**,** 1531-68.
TRAUTMANN, E. M., HESSE, J. K., STINE, G. M., XIA, R., ZHU, S., O'SHEA, D. J., KARSH, B., COLONELL, J., LANFRANCHI, F. F., VYAS, S., ZIMNIK, A., STEINMANN, N. A., WAGENAAR, D. A., ANDREI, A., LOPEZ, C. M., O'CALLAGHAN, J., PUTZEYS, J., RADUCANU, B. C., WELKENHUYSEN, M., CHURCHLAND, M., MOORE, T., SHADLEN, M., SHENOY, K., TSAO, D., DUTTA, B. & HARRIS, T. 2023. Large-scale high-density brain-wide neural recording in nonhuman primates. *bioRxiv***,** 2023.02.01.526664.
TREPKA, E. B., ZHU, S. D., XIA, R. B., CHEN, X. M. & MOORE, T. 2022. Functional interactions among neurons within single columns of macaque V1. *Elife,* 11.
TS'O, D. Y., GILBERT, C. D. & WIESEL, T. N. 1986. Relationships between horizontal interactions and functional architecture in cat striate cortex as revealed by cross-correlation analysis. *J Neurosci,* 6**,** 1160-70.
USREY, W. M., REPPAS, J. B. & REID, R. C. 1998. Paired-spike interactions and synaptic efficacy of retinal inputs to the thalamus. *Nature,* 395**,** 384-7.
VAN KERKOERLE, T., SELF, M. W., DAGNINO, B., GARIEL-MATHIS, M. A., POORT, J., VAN DER TOGT, C. & ROELFSEMA, P. R. 2014. Alpha and gamma oscillations characterize feedback and feedforward processing in monkey visual cortex. *Proc Natl Acad Sci U S A,* 111**,** 14332-41.
VAN KERKOERLE, T., SELF, M. W. & ROELFSEMA, P. R. 2017. Layer-specificity in the effects of attention and working memory on activity in primary visual cortex. *Nat Commun,* 8**,** 13804.
VANGENEUGDEN, J., VAN BEEST, E. H., COHEN, M. X., LORTEIJE, J. A. M., MUKHERJEE, S., KIRCHBERGER, L., MONTIJN, J. S., THAMIZHARASU, P., CAMILLO, D., LEVELT, C. N., ROELFSEMA, P. R., SELF, M. W. & HEIMEL, J. A. 2019. Activity in Lateral Visual Areas Contributes to Surround Suppression in Awake Mouse V1. *Curr Biol,* 29**,** 4268-4275 e7.
VON DER HEYDT, R. 2015. Figure-ground organization and the emergence of proto-objects in the visual cortex. *Frontiers in Psychology,* 6**,** 1695.
VON DER HEYDT, R. 2023. Visual cortical processing—From image to object representation. *Frontiers in Computer Science,* 5.
VON DER HEYDT, R., PETERHANS, E. & BAUMGARTNER, G. 1984. Illusory contours and cortical neuron responses. *Science,* 224**,** 1260-2.
WAGATSUMA, N., HU, B., VON DER HEYDT, R. & NIEBUR, E. 2021. Analysis of spiking synchrony in visual cortex reveals distinct types of top-down modulation signals for spatial and object-based attention. *PLoS Comput Biol,* 17**,** e1008829.
WALKER, G. A., OHZAWA, I. & FREEMAN, R. D. 1999. Asymmetric suppression outside the classical receptive field of the visual cortex. *J Neurosci,* 19**,** 10536-53.
WEBB, B. S., TINSLEY, C. J., BARRACLOUGH, N. E., PARKER, A. & DERRINGTON, A. M. 2003. Gain control from beyond the classical receptive field in primate primary visual cortex. *Vis Neurosci,* 20**,** 221-30.
WILLIFORD, J. R. & VON DER HEYDT, R. 2016. Figure-Ground Organization in Visual Cortex for Natural Scenes. *eNeuro,* 3.
YAN, Y., ZHAOPING, L. & LI, W. 2018. Bottom-up saliency and top-down learning in the primary visual cortex of monkeys. *Proc Natl Acad Sci U S A,* 115**,** 10499-10504.
ZARELLA, M. D. & TS'O, D. Y. 2016. Cue combination encoding via contextual modulation of V1 and V2 neurons. *Eye Brain,* 8**,** 177-193.
ZHANG, N. R. & VON DER HEYDT, R. 2010. Analysis of the context integration mechanisms underlying figure-ground organization in the visual cortex. *Journal of Neuroscience,* 30**,** 6482-6496.
ZHANG, S., XU, M., KAMIGAKI, T., HOANG DO, J. P., CHANG, W. C., JENVAY, S., MIYAMICHI, K., LUO, L. & DAN, Y. 2014. Selective attention. Long-range and local circuits for top-down modulation of visual cortex processing. *Science,* 345**,** 660-5.

ZHAOPING, L. 2005. Border ownership from intracortical interactions in visual area v2. *Neuron,* 47**,** 143-53.

ZHOU, H., FRIEDMAN, H. S. & VON DER HEYDT, R. 2000. Coding of border ownership in monkey visual cortex. *J Neurosci,* 20**,** 6594-611.

ZHU, S. D., ZHANG, L. A. & VON DER HEYDT, R. 2020. Searching for object pointers in the visual cortex. *Journal of Neurophysiology,* 123**,** 1979-1994.

ZIPSER, K., LAMME, V. A. & SCHILLER, P. H. 1996. Contextual modulation in primary visual cortex. *J Neurosci,* 16**,** 7376-89.

Table S1. Number of neurons selective to B_{own} (LC) across recordings.

Layer	Total	p_{Side} <0.05		p_{Side} ≥0.05		Layer	Total	p_{Side} <0.05		p_{Side} ≥0.05	
		p_{LC} ≥0.05	p_{LC} <0.05	p_{LC} <0.05	p_{LC} ≥0.05			p_{LC} ≥0.05	p_{LC} <0.05	p_{LC} <0.05	p_{LC} ≥0.05
	***pen*1**						***pen2***				
2/3	29	6	5	6	12	2/3	55	1	14	18	22
4A/B	19	0	5	8	6	4A/B	34	0	7	10	17
4C	38	3	7	16	12	4C	54	4	15	22	13
5/6	40	2	7	18	13	5/6	27	5	2	4	16
	pen3						***pen4***				
2/3	15	1	1	4	9	2/3	0	0	0	0	0
4A/B	27	0	4	9	14	4A/B	34	3	0	2	29
4C	60	1	12	24	23	4C	60	2	4	5	49
5/6	40	2	7	2	29	5/6	37	3	0	2	32
	pen all										
2/3	99	8	20	28	43						
4A/B	114	3	16	29	66						
4C	212	10	38	67	97						
5/6	144	12	16	26	90						

Table S2. Comparison of CCG asymmetries during CRF and nCRF for each recording.

4C-2/3	*CRF*	*nCRF*	**Δ**	***p***	**4A/B-2/3**	*CRF*	*nCRF*	**Δ**	***p***
*pen*1	0.036	-0.004	-0.040	$2.8*10^{-7}$	*pen*1	0.046	-0.005	-0.050	$7.5*10^{-12}$
pen2	0.037	0.013	-0.024	$3.7*10^{-9}$	*pen2*	0.030	0.022	-0.008	0.066
pen3	0.017	0.033	0.016	0.29	*pen3*	0.049	0.052	0.003	0.99
4C-5/6	*CRF*	*nCRF*	**Δ**	***p***	**4A/B-5/6**	*CRF*	*nCRF*	**Δ**	***p***
*pen*1	-0.010	-0.044	-0.033	0.0015	*pen*1	0.012	-0.028	-0.040	$2.1*10^{-6}$
pen2	-0.009	-0.027	-0.018	$1.5*10^{-5}$	*pen2*	-0.011	-0.018	-0.007	0.059
pen3	-0.036	-0.062	-0.026	$5.8*10^{-7}$	*pen3*	-0.025	-0.087	-0.063	$9.1*10^{-15}$
pen4	-0.041	-0.093	-0.051	$3.1*10^{-8}$	*pen4*	-0.030	-0.089	-0.060	$9.1*10^{-12}$

Table S3. GLMs for dependence of border ownership and local contrast on CCG asymmetry.

$$B_{own}(pair) \sim 1 + CCG\ asymmetry + \ laminar\ combination + pen$$

$$LC(pair) \sim 1 + CCG\ asymmetry + \ laminar\ combination + pen$$

GLM	Border ownership (B_{own})				Local contrast (LC)			
	Estimate	SE	tStat	p	Estimate	SE	tStat	p
Intercept	0.166	0.008	21.379	0	0.362	0.010	35.352	0
CCG asymmetry	**-0.158**	0.032	-4.880	**$1.1*10^{-6}$**	**-0.044**	0.043	-1.037	**0.300**
4C-5/6 *rel.4C-2/3*	0.014	0.007	1.948	0.05	-0.117	0.009	-12.606	$3.5*10^{-35}$
4A/B-2/3 *rel.4C-2/3*	$2.5*10^{-5}$	0.006	0.004	0.99	-0.016	0.008	-1.877	0.061
4A/B-5/6 *rel.4C-2/3*	0.009	0.007	1.351	0.18	-0.136	0.009	-15.093	0
pen2 rel.pen1	-0.009	0.007	-1.219	0.22	0.010	0.010	0.980	0.327
pen3 rel.pen1	0.038	0.009	4.435	$9.7*10^{-6}$	0.035	0.011	3.082	0.002
pen4 rel.pen1	0.049	0.010	5.147	$2.9*10^{-7}$	-0.088	0.013	-6.910	$6.4*10^{-12}$

Number of observations: 2118; Error degrees of freedom: 2110

GLM(B_{own}): R^2=0.11; F-statistic vs. constant model: 37.2, p-value=0.

GLM(LC): R^2=0.27; F-statistic vs. constant model: 109, p-value=0.

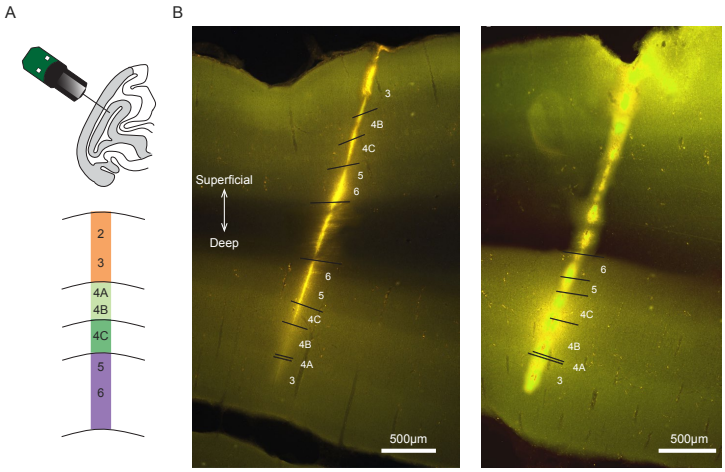

Supplementary Figure S1. Histological data for Neuropixels recordings in macaque V1. (A) Neuropixels probe (384 channels/3.84mm) penetrations made into the lateral surface or underlying calcarine sulcus of macaque V1. Bottom: Diagram of designated laminar compartments. (B) Histological reconstruction of probe tracks based on DiI derivative staining for two example recordings (*pen3-4*). Here, Neuropixels probes passed through the lateral surface and reached the calcarine sulcus of V1. Only neurons in the calcarine V1 from these two recordings were tested and included in the analysis. Designated boundaries are shown. Scale bar, 500 µm.

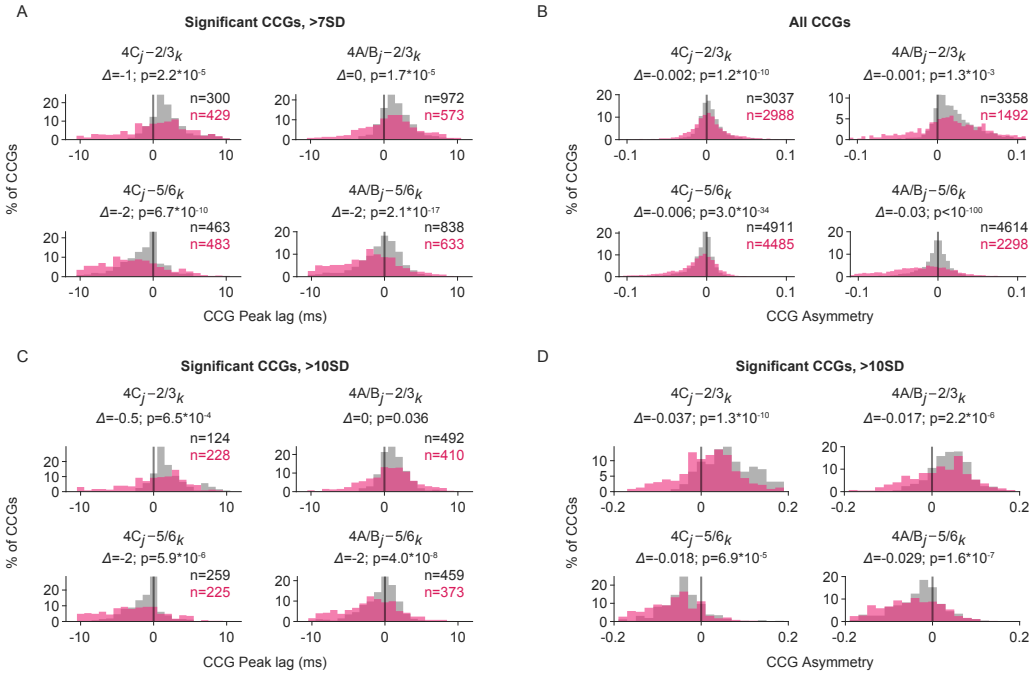

Supplementary Figure S2. Comparison of interlaminar cross-correlations during CRF and nCRF stimulation under different CCG criteria. (A) Histogram distributions of CCG peak lags for each of the four key interlaminar combinations in the combined dataset during CRF (gray) and nCRF (magenta) stimulation. The shift (Δ) in median CCG peak lags during nCRF stimulation relative to CRF stimulation is shown. Significant CCGs are defined as those with peaks exceeding 7 SD above the noise level (flank). (B) Similar to (A), but comparing CCG asymmetry across all CCGs, including both significant and non-significant ones. (C) Comparison of CCG peak lags using a stricter criterion, where significant CCGs are defined as those with peaks exceeding 10 SD above the noise level (flank). (D) Comparison of CCG asymmetry using the stricter criterion of 10 SD.